

SYRACUSE UNIV N Y DEPT OF CHEMICAL ENGINEERING AND --ETC F/G 20/11
ELASTIC-PLASTIC DEFORMATION IN CRACKED SOLIDS AND DUCTILE FRACT--ETC(U)
JAN 82 H W LIU DAAG29-78-G-0069

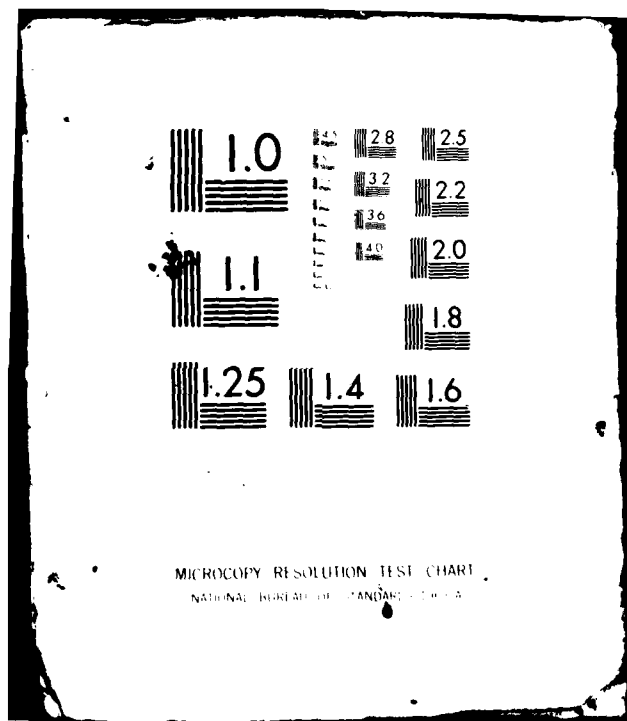
UNCLASSIFIED

ARO-15226.3-E

NL

1.4.1
A.
Δ 0.80%

END
DATE
FILMED
3 82
DTIC



UNCLASSIFIED
SECURITY CLASSIFICATION OF THIS PAGE (When Data Entered)

LEVEL III

12

AD A110805

REPORT DOCUMENTATION PAGE		
1. REPORT NUMBER 15226.3-E	2. GOVT ACCESSION NO. A110805 H045905	3. RECIPIENT'S CATALOG NUMBER
4. TITLE (and Subtitle) Elastic-Plastic Deformation in Cracked Solids and Ductile Fracture Criterion		5. TYPE OF REPORT & PERIOD COVERED Final: 1 Jun 78 - 31 Dec 81
6. AUTHOR(s) H. W. Liu		7. PERFORMING ORG. REPORT NUMBER
8. CONTRACT OR GRANT NUMBER(s) DAAG29 78 G 0069		9. PROGRAM ELEMENT, PROJECT, TASK AREA & WORK UNIT NUMBERS
10. CONTROLLING OFFICE NAME AND ADDRESS Syracuse University Syracuse, NY 13210		11. REPORT DATE Jan 82
12. MONITORING AGENCY NAME & ADDRESS (if different from Controlling Office)		13. NUMBER OF PAGES 66
14. SECURITY CLASS. (of this report) Unclassified		15. DECLASSIFICATION/DOWNGRADING SCHEDULE

16. DISTRIBUTION STATEMENT (of this Report)

Approved for public release; distribution unlimited.

17. DISTRIBUTION STATEMENT (of the abstract entered in Block 20, if different from Report)

NA

18. SUPPLEMENTARY NOTES

The view, opinions, and/or findings contained in this report are those of the author(s) and should not be construed as an official Department of the Army position, policy, or decision, unless so designated by other documentation.

19. KEY WORDS (Continue on reverse side if necessary and identify by block number)

cracking(fracturing) stresses
fracture properties strain fields
fatigue(materials)
crack propagation

20. ABSTRACT (Continue on reverse side if necessary and identify by block number)

The main objectives of the program are to study crack tip stresses and crack tip deformation, and to use the findings of these studies to investigate the fractures of ductile and tough materials. Crack tip displacement and strain fields were measured with the moire method, and the crack tip stress, displacement, and strain fields were calculated with the finite elements method. The measured displacement and strain fields agree well with the finite element calculations. The results were used to develop the direct correspondence method of evaluating fracture toughness of ductile tough materials and were also to analyze deformation mode of fatigue crack growth.

DD FORM 1 JAN 73 1473 EDITION OF 1 NOV 65 IS OBSOLETE

UNCLASSIFIED

SECURITY CLASSIFICATION OF THIS PAGE (When Data Entered)

02 08 250

DTIC FILE COPY

DTIC
ELECT
FEB 11 1982

ELASTIC-PLASTIC DEFORMATION IN CRACKED SOLIDS AND DUCTILE FRACTURE CRITERION

H. W. Liu
Syracuse University
Department of Chemical Engineering and Materials Science
Syracuse, New York 13210

FINAL REPORT

ARMY RESEARCH OFFICE
Research Triangle Park, North Carolina

Contract No.: DAHC04-74-G-0165
DAA629-76-G-0290
DAAG29--78-G-0069

July 1, 1975 - December 30, 1981

Accession For	
NTIS GRA&I	<input checked="" type="checkbox"/>
DTIC TAB	<input type="checkbox"/>
Unannounced	<input type="checkbox"/>
Justification	
By	
Distribution/	
Availability Codes	
Dist	Avail and/or Special
A	



Office of Sponsored Programs
Syracuse University
January 1981

The main objectives of the program are to study crack tip stresses and crack tip deformation, and to use the findings of these studies to investigate the fractures of ductile and tough materials.

Crack tip displacement and strain fields were measured with the moire method, and the crack tip stress, displacement, and strain fields were calculated with the finite elements method. The measured displacement and strain fields agree well with the finite element calculations. The results were used to develop the direct correspondence method of evaluating fracture toughness of ductile and tough materials and were also used to analyze deformation mode of fatigue crack growth.

Griffith⁽¹⁾ formulated his well known energy criterion for brittle fractures. At the fracture initiation of a cracked brittle solid in the condition of fixed grip, the release rate of the stored strain energy equals or exceeds the dissipative surface energy rate. $\partial U_e / \partial a \geq \partial U_s / \partial a = 2\gamma$, where U_e and U_s are strain energy and surface energy; γ , the surface energy per unit area; and a , crack length. γ is constant for a given material. Assuming a constant dissipative rate of plastic energy Γ , Irwin⁽²⁾ and Orowan⁽³⁾ extended the energy criterion to metallic solids, where plastic deformation takes place at crack tips.

The crack tip elastic stresses, strains, and displacements are characterized by the stress intensity factor, K . Liu⁽⁴⁾ has shown that for the case of small scale yielding, SSY, K characterizes crack tip stresses, strains, and displacements even within a crack tip plastic zone in a metallic specimen. Liu has emphasized that the capability of K to characterize crack tip stresses, strains and displacements forms the fundamental basis of the linear elastic fracture mechanics rather than the global energy balance.

More recently, Hutchinson⁽⁶⁾, and Rice and Rosengren⁽⁷⁾ derived the characteristic crack tip stress, strain and displacement fields in power law strain hardening materials. The crack tip stress, strain and displacement fields can be characterized by J , which is a contour independent integral. J is also the rate of potential energy change during the cracking process in a non-linear elastic solid. J has been widely used to study non-linear fracture mechanics. However, the characteristic crack tip fields are not universally valid. Figure 1 shows the slip line fields of a double-edge-notched specimen and a center-notched specimen under fully plastic tensile loads. Because of the difference in in-plane constraints, the principle tensile stress equal to $(2 + \pi)k$ in one case and $2k$ in the other; k is the yield stress in terms of shear. The characteristic flow fields and stress fields of these two cases are grossly different. In other words, for different types of specimen geometry, the characteristic fields might be different. The same J -value might mean different crack tip stresses, strains, and displacements. As a result, one would expect that specimens of different geometric types would fail at different J -values. Indeed, Hancock and Cowling⁽⁸⁾ tested specimens of five different geometries, Fig. 2. The lowest and the highest values of crack tip opening displacements at fracture, δ_c , differ by a factor of 10. δ is related to J but the relation differs for different flow fields. Taking the difference of the flow fields into consideration Hancock and Cowling⁽⁸⁾ found the corresponding extreme values of J_c to be 570 kNm^{-1} and 147 kNm^{-1} , a difference of a factor of four.

Compact tension specimens and three point bending specimens were extensively used to measure fracture toughnesses of a number of tough and ductile materials. Yet according to the results shown in Fig. 2, the measured J_{IC} values would be overvalued in comparison with the deeply double-edge-cracked specimens.

In view of the divergent results of recent findings, a sound and rational method of fracture-toughness evaluation is badly needed. This research program follows a much more careful process of development. The crack tip deformations were measured and calculated numerically. The measurements and the numerical calculations were compared with the analytical results. Based on these studies, the characteristic crack tip fields were deduced. Then the direct correspondence method of evaluating fracture toughnesses was developed.

Three characteristic two-dimensional crack models exist: plane strain, plane stress and Dugdale model. The characteristic crack tip fields of plane stress and Dugdale models were studied extensively in this investigation. The crack tip stress, strain and displacement fields of a small sample in large scale yielding or general yielding correspond directly to the crack tip fields of a large sample in small scale yielding. Therefore these two samples, one small and one large, must have the same K or J value. This conclusion is substantiated by the excellent agreement between the measured crack tip strain and displacement fields with the finite element method calculations; the excellent agreement between the finite element calculations and the analytical results of Hutchinson⁽⁶⁾ and Rice and Rosengren⁽⁷⁾; and the agreement of the measured and calculated load-elongation curves of cracked samples. The choice of a specific model and specific mechanical parameter for fracture toughness evaluation is heavily dependent on the specimen thickness. The details are summarized in Appendix I: "Thickness Effects on the Choice of Fracture Criteria".

At times, the extensive experimental and theoretical studies appear to be overly cautious. However, in view of the recent work by Hancock and Cowling⁽⁸⁾, our careful approach is warranted. The method of direct correspondence is extremely promising for the future development of non-linear fracture mechanics.

Fatigue cracks in ductile materials are often propagated by shear deformation process. When a crack is small and the applied stress approaches the tensile yield stress of a material, the crack tip plastic zone size will be comparable or even larger than the crack length. The effects of large scale yielding will certainly make the correlation between ΔK and da/dN invalid. Crack tip shear deformation in both small scale yielding and large scale yielding were calculated. Again the principle of direct correspondence is used to establish the equivalent K-value of a micro-crack in large scale yielding. The results were used to analyze fatigue crack growth.

Materials are not homogeneous. They consist of weak and soft phases and strong and hard phases. The crack tip shear decohesion displacement in a soft phase was calculated. The shear deformation at the crack tip in a soft phase is constrained by the neighboring hard phase. The calculated shear deformations were used to analyze fatigue crack growth. The analyses on micro-crack and the heterogeneous two-phase materials are summarized in Appendix II, "Crack Tip Deformation and Fatigue Crack Growth."

The list of publications on the research results of this program is shown in Appendix III.

The grant has supported three graduate students: Drs. Wan-liang Hu, C. Y. Yang and Mr. Chien-Erh Hong. Mr. Hong has yet to complete his thesis. Their dissertation and thesis titles and present affiliations are given in Appendix IV.

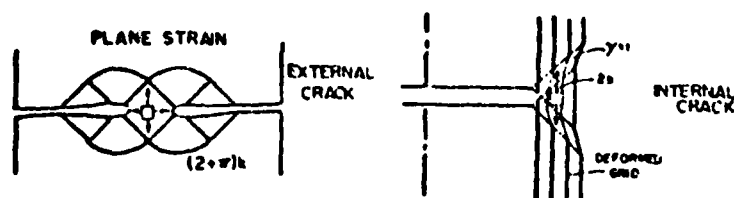


Fig. 1 Slip line fields for fully plastic tension mode - plane strain.

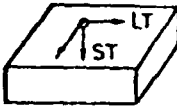
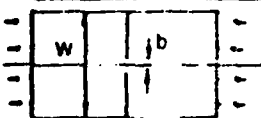
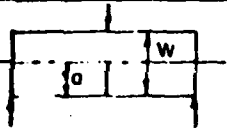
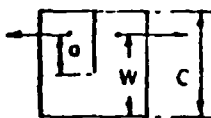
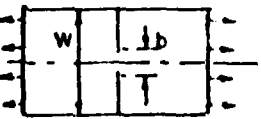
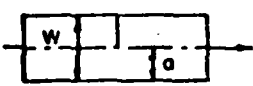
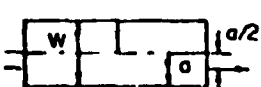
COD AT CRACK EXTENSION δ_1			
MATERIAL: HYBO (LT)			
YIELD STRESS: 560 MNm^{-2} (80 KSI)			
			
SPECIMEN	TYPE	DIMENSIONS	$\delta_1, \mu\text{m}$
	IO I DEC	$W = 10b = 50 \text{ mm}$	90
	3 PB	$W = 2a = 25 \text{ mm}$	170
	CTS	$W = 2a = 50 \text{ mm}$ $C = 1.25 W$	170
	4 I DEC	$W = 4b = 50 \text{ mm}$	302
	SEN LOADED OVER CRACK TIP	$W = 2a = 10 \text{ mm}$	450
	SEN LOADED IN CENTRE OF LIGAMENT	$W = 2a = 20 \text{ mm}$	900

Fig. 2 Crack tip openings at fracture initiation in range of specimen geometries (Ref. 8).

REFERENCES

1. Griffith, A. A., "The Phenomena of Rupture and Flow in Solids," Philosophical Transactions of the Royal Society (London) Series A, Vol. 221, 1921, pp. 163-198.
2. Irwin, G. R., "Fracture Dynamics," Fracturing of Metals, Am. Society for Metals (Cleveland) 1948, pp. 147-166.
3. Orowan, E., "Energy Criteria of Fracture," Welding Research Supplement, Vol. 20, 1955, p. 1575.
4. Liu, H. W., "Discussion to 'A Critical Appraisal of Fracture Mechanics,'" STP 381, ASTM-NASA, 1965, pp 23-26.
5. Liu, H. W., "Fracture Criteria of Cracked Metallic Plate," International Journal of Fracture Mechanics, Vol. 2, 1966, pp. 393-399.
6. Hutchinson, J. W., "Singular Behavior at the End of a Tensile Crack in a Hardening Material," J. of Mech. and Phys. of Solids, Vol. 16, 1968, p. 13.
7. Rice, J. R. and Rosengren, G. F., "Plane Strain Deformation Near a Crack Tip in a Power-Law Hardening Material," J. of Mech. and Phys. of Solids Vol. 16, 1968, p. 1.
8. Hancock, J. W. and Cowling, M. J., "Role of State of Stress in Crack-tip Failure Processes," Metal Science, Aug.-Sept., 1980, pp. 293-304.

APPENDIX I

THICKNESS EFFECTS ON THE CHOICE
OF FRACTURE CRITERIA

by

H. W. Liu*

Wan-liang Hu**

Albert S. Kuo***

Presented at the
ASTM Second International Symposium
on
Elastic-Plastic Fracture Mechanics

Philadelphia, PA
October 6-9, 1981

*Syracuse University
**Hanford Engineering Development Laboratory, Westinghouse Corporation
***Fairchild Republic Company

ABSTRACT

The stresses and strains in a cracked solid are in a complicated 3-dimensional state. There are three two-dimensional limiting cases: plane strain, plane stress, and Dugdale's strip yielding case. The thickness of a plate relative to crack tip plastic zone size determines which one of these three limiting cases is predominant. The characteristics of the plane stress and the Dugdale strip yielding crack tip fields were investigated with the moire method together with the finite element calculations. The state of the crack tip stress and strain fields approaches that of plane strain for very thick plates. For a very thin plate with a very large crack tip plastic zone, the Dugdale's strip yielding model is applicable, and the crack opening displacement, crack tip opening displacement, and thickness contraction are related to K or J and they can be used for fracture toughness measurements. When a plate thickness is in between these two extremes, there exists a characteristic plane stress crack tip field. The correspondence of the plane stress crack tip fields in small scale yielding and in general yielding was established, and the J -value of a sample in general yielding can be obtained from the established correspondence. The value of the applied J -field of a small sample in general yielding can be measured in terms of the applied stress and the specimen elongation

Keywords: Non-linear fracture mechanics, fracture toughness, small scale yielding, general yielding, COD, CTOD, K , J , and thickness contraction.

exist. Still further away is Region IV, where the effects of specimen geometry and type loading dominate the deformation characteristics. Note that, in general, not all of these four regions are present. For example, Region III diminishes with increasing load. For a very thick single-edge-cracked, SEN, specimen, only Region I and Region IV may exist.

The nature of the plane strain stiffening effect in Region I has been discussed previously^[10]. It is the stresses and strains in the immediate vicinity of the crack tip within the stiffened zone that cause fracture initiation. The crack tip stiffened zone is embedded within the plane stress crack tip field. It is reasonable that the stresses and strains in the stiffened zone should be characterized by the intensity of the plane stress crack tip field. In other words, the same intensity of the plane stress crack tip field infers the same stresses and strains in the stiffened zone, even though the exact values of the stresses and strains in the stiffened zone are unknown. Therefore, the intensity of the plane stress crack tip field also characterizes the condition for crack initiation. The degree of the crack tip strengthening is affected by plate thickness, therefore this conclusion is applicable only to samples of same thickness. We will focus our attention in Regions II and III.

Crack tip stresses, strains and displacements in elastic solids can be expressed in terms of the stress intensity factor K. In a like manner, Hutchinson^[8] and Rice and Rosengren^[9] have shown that crack tip stresses, strains, and displacements can be expressed in terms of J.

$$\begin{aligned}
 [\sigma_{ij}, \sigma_e] &= \sigma_0 \left[\frac{J}{\alpha \sigma_0 \epsilon_0 I_n r} \right]^{\frac{1}{n+1}} [\tilde{\sigma}_{ij}(\theta, n), \tilde{\sigma}_e(\theta, n)] \\
 \epsilon_{ij} &= \alpha \epsilon_0 \left[\frac{J}{\alpha \sigma_0 \epsilon_0 I_n r} \right]^{\frac{n}{n+1}} \tilde{\epsilon}_{ij}(\theta, n) \\
 u_i - u_i^0 &= \alpha \epsilon_0 \left[\frac{J}{\alpha \sigma_0 \epsilon_0 I_n} \right]^{\frac{n}{n+1}} r^{\frac{1}{n+1}} \tilde{u}_i(\theta, n)
 \end{aligned} \tag{1}$$

II. CHARACTERISTIC PLANE STRESS CRACK TIP FIELD - SMALL SCALE YIELDING AND LARGE SCALE YIELDING CORRESPONDENCE

Crack tip strains, ϵ_{yy} , were measured by Gavigan, Ke and Liu^[7] in double-edge-cracked, DEN, specimens made of three batches of 2024-0 aluminum alloy. 102 mm and 203 mm (4 or 8 inches) wide specimens of three different thicknesses were tested. The measurements are shown in Fig. 1. The solid lines are plane-stress finite element calculations. Away from the crack tip, in the region $r > t$, the measurements and the calculations agree very well. Close to the crack tip, $r < t$, the measured strains are less than the calculated values. These strains were measured on the specimen surface; however the surface was not free to deform, because the surface was coupled to the interior of the specimen, where "plane strain" constraint existed. The constraint "stiffened" the crack tip area and it reduced strains on the surface. The constraint is a localized three-dimensional phenomenon. Beyond the crack tip stiffened zone, the measurements clearly indicate the existence of a characteristic plane stress crack tip field. Figure 2 shows the measured and the calculated load-displacement, $P-\Delta$, curves. Again, the agreement of the measurements and the calculations is very good.

Figure 3 schematically shows various regions of stress and strain fields. Region I extends from the crack tip to a distance approximately equal to half of the specimen thickness. In this region, the plane strain stiffening effect exists, and the three dimensional effect is clearly shown. In Region II, the plane stress condition prevails. The stress and strain fields approach the analytical results of Hutchinson^[8] and Rice and Rosengren^[9]*. Region III lies further away from the crack tip where the material deforms elastically and the stresses and strains vary with $r^{-0.5}$. The measurements shown in Fig. 1 were all made at general yielding. However if a specimen is large enough, the characteristic elastic field may

*This will be discussed in detail later.

exist. Still further away is Region IV, where the effects of specimen geometry and type loading dominate the deformation characteristics. Note that, in general, not all of these four regions are present. For example, Region III diminishes with increasing load. For a very thick single-edge-cracked, SEN, specimen, only Region I and Region IV may exist.

The nature of the plane strain stiffening effect in Region I has been discussed previously^[10]. It is the stresses and strains in the immediate vicinity of the crack tip within the stiffened zone that cause fracture initiation. The crack tip stiffened zone is embedded within the plane stress crack tip field. It is reasonable that the stresses and strains in the stiffened zone should be characterized by the intensity of the plane stress crack tip field. In other words, the same intensity of the plane stress crack tip field infers the same stresses and strains in the stiffened zone, even though the exact values of the stresses and strains in the stiffened zone are unknown. Therefore, the intensity of the plane stress crack tip field also characterizes the condition for crack initiation. The degree of the crack tip strengthening is affected by plate thickness, therefore this conclusion is applicable only to samples of same thickness. We will focus our attention in Regions II and III.

Crack tip stresses, strains and displacements in elastic solids can be expressed in terms of the stress intensity factor K . In a like manner, Hutchinson^[8] and Rice and Rosengren^[9] have shown that crack tip stresses, strains, and displacements can be expressed in terms of J .

$$\begin{aligned} [\sigma_{ij}, \sigma_e] &= \sigma_0 \left[\frac{J}{\alpha \sigma_0 \epsilon_0 I_n r} \right]^{\frac{1}{n+1}} [\tilde{\sigma}_{ij}(\theta, n), \tilde{\sigma}_e(\theta, n)] \\ \epsilon_{ij} &= \alpha \epsilon_0 \left[\frac{J}{\alpha \sigma_0 \epsilon_0 I_n r} \right]^{\frac{n}{n+1}} \tilde{\epsilon}_{ij}(\theta, n) \\ u_i - u_i^0 &= \alpha \epsilon_0 \left[\frac{J}{\alpha \sigma_0 \epsilon_0 I_n r} \right]^{\frac{n}{n+1}} \frac{1}{r^{\frac{1}{n+1}}} \tilde{u}_i(\theta, n) \end{aligned} \quad (1)$$

I. INTRODUCTION

Griffith^[1] formulated the energy fracture criterion for brittle solids. At the onset of fracture initiation, the driving force (i.e. the rate of change of the elastic strain energy of a cracking solid), is equal to the energy dissipation rate (i.e. the surface energy of a brittle solid), which is a constant. Irwin^[2] and Orowan^[3] extended the Griffith energy criterion to metallic solids by assuming the plastic energy dissipation rate for fracture initiation was a material constant. However, it can be shown that the plastic energy dissipation rate of a cracking infinite plate in the condition of plane strain is linearly proportional to crack length, $2a$. So does the rate of change of the elastic strain energy of the plate. The fracture criterion of the global energy balance leads to a constant fracture stress for an infinite plate. The fracture stress is independent of crack length. This conclusion contradicts the experimental evidences, therefore the criterion of the global energy balance for fracture initiation without the consideration of the detailed fracture processes, must be fortuitous^[4,5].

Liu^[4,5] has shown that the stress intensity factor, K , characterizes crack tip stresses and strains even within the crack tip plastic zone, r_p , if the condition of small scale yielding, SSY, is satisfied. The very existence of this conclusion allows us to determine experimentally the minimum specimen size for valid fracture toughness measurements. But the condition of SSY is a sufficient, not the necessary, condition for the validity of the linear elastic fracture mechanics. The necessary condition is that K should be able to characterize the crack tip stress or strain responsible for the defined fracture process. When the applied stress or strain at the fracture process zone reaches the critical value, fracture will occur.

If it is limited to the realm of the linear elastic fracture mechanics, with the restriction to the same fracture mode and the limitation to the same thickness, the concept of the K -characterization of the crack tip field and the assumption of

the constant dissipation rate of plastic deformation energy lead to the same results. However, when it is extended beyond the realm of the LEFM, only the correct analysis will lead to the desired results. The concept of characterizing crack tip stress and strain fields by the stress intensity factor, K , forms a sound basis for the extension of the LEFM to non-linear fracture mechanics. This paper illustrates its applications.

The characteristic crack tip stresses and strains are greatly affected by specimen thickness. When a small plastic zone at a crack tip is imbedded in a massive and thick plate, the constraint to thickness contraction induces a state of high triaxial stresses, and the state of the crack tip field approaches that of plane strain. The maximum principle stress, σ_{\max} is nearly $2.45 \times \sigma_{\text{flow}}$, and the triaxial state of stresses restrains plastic deformation. On the other hand, a very large plastic zone in a thin plate causes crack tip necking. In this instance, extensive plastic deformation is concentrated within a thin narrow strip. Within the strip, the plate thickness contracts considerably, and the deformation approaches the Dugdale strip yielding model^[6]. When specimen thickness is intermediate between these two extremes, a characteristic plane stress crack tip field exists. In this case, the maximum principle stress is nearly equal to σ_{flow} .

Fracture processes are controlled by the crack tip stresses and strains which are greatly affected by plate thickness. Therefore the choice of the fracture criteria must also be dependent on plate thickness.

This paper summarizes and synthesizes the experimental and theoretical work on the effects of thickness on crack tip stresses, on crack tip deformation, and on the choice of the fracture criteria for non-linear fracture mechanics. Plate thicknesses less than that of plane strain were studied. The results are applicable to structures made of high toughness materials which are less than 2 inches thick.

for a material with a power law stress-strain relation

$$\frac{\epsilon}{\epsilon_0} = \alpha \left(\frac{\sigma}{\sigma_0} \right)^n \quad (2)$$

where, σ_0 is the flow stress at the strain ϵ_0 . When $\sigma_0 = \sigma_Y$ and $\epsilon_0 = \epsilon_Y$, $\alpha = 1$. $n \geq 1$. σ_e is effective stress. $\tilde{\sigma}_{ij}(\theta, n)$, $\tilde{\sigma}_e(\theta, n)$, $\tilde{\epsilon}_{ij}(\theta, n)$ and $\tilde{u}_i(\theta, n)$ are functions of θ and n . They define the distributions of their corresponding components in the θ -direction. $I_n(n)$ is a function of n .

$$I_n = \int_{-\pi}^{\pi} \left[\frac{n}{n+1} \tilde{\sigma}_e^{(n+1)} + () \right] d\theta \quad (3)$$

J is the well known J-integral. It characterizes crack tip stresses, strains, and displacements analogous to K for elastic solids.

For a non-linear elastic solid, J can also be considered as the rate of the change of the potential energy with respect to crack increment. In the case of SSY,

$$J = G = \frac{K^2}{\bar{E}} \quad (4)$$

where $\bar{E} = E$ for plane stress and $\bar{E} = E/(1-\nu^2)$ for plane strain. ν is the Poisson's ratio.

However, the characteristic crack tip fields given by Eqn. (1) are not universally valid in all the cases. Figure (4) shows the slip line fields of a double-edge-notched specimen and a single-edged-notched specimen under fully plastic tensile loads. Because of the difference in in-plane constraint, the principle tensile stress equal to $(2 + \pi)k$ in one case and $2k$ in the other; k is the yield stress in terms of shear. The characteristic flow fields and stress fields of these two cases are grossly different. In other words, for different types of specimen geometry, the characteristic fields might be different. The same

J-value might indicate different crack tip stresses, strains, and displacements. As a result, one would expect that specimens of different geometric types would fail at different J-values. Indeed, Hancock and Cowling^[11] tested specimens of five different geometries. The lowest and the highest values of crack tip opening displacements at fracture, δ_c differ by a factor of 10. δ is related to J but the relation differs for different flow fields. Taking the difference of the flow fields into consideration Hancock and Cowling^[11] found the corresponding extreme values of J_c to be 570 kNm^{-1} and 147 kNm^{-1} , a difference of a factor of four.

In order to measure fracture toughness as a material property, a reference state of crack tip field must be established. The most meaningful one is that of the small scale yielding. With this choice, the measured fracture toughness of a small sample in general yielding will be able to predict the fracture strength of a large structure in small scale yielding.

Plane stress calculations are also made for the double-edge-cracked sample and the single-edge-cracked sample in SSY, LSY, and GY. The characterization of the crack tip fields, the correspondence between the crack tip fields in the state of the SSY, LSY and GY, and their relation to the applied stress and the imposed elongation are studied.

The crack tip stress and strain fields in samples made of two batches of aluminum alloy in the state of SSY were studied using plane stress finite analysis. A circular sample with a crack along one of the radial lines and with boundary displacements given by the dominant terms of the linear elastic solution, i.e. $u_i = (K/2\mu)(r/2\pi)^{1/2} \tilde{u}_i(\theta)$, serves as the reference state, see Fig. 5. μ is shear modulus. The $\sigma - \epsilon$ relations are prescribed by $\sigma = E\epsilon$ for $\sigma \leq \sigma_y$ and $\sigma = k\epsilon^N$

for $\sigma \geq \sigma_Y$. $k = E \sigma_Y^{1-N}$. $\sigma_Y = 69$ MPa (10 ksi) and $N = 0.22$ for batch B; and $\sigma_Y = 50$ MPa (7.26 ksi) and $N = 0.315$ for batch C. The finite element mesh is shown in Fig. 5. The details of the calculations are given in Ref. 12. The crack line stresses and strains for batch C aluminum are shown in the dimensionless plots in Fig. 6. The results of nine loading steps are shown. The value of K_I ranges from 1.24 to 4.4 MPa \sqrt{m} (1.25 to 4 ksi \sqrt{in}).

Within r_p , the y -direction strain and stress can be expressed as

$$\epsilon_{yy} = \epsilon_{yy}(r=r_p) \left(\frac{r_p}{r}\right)^m = \frac{\epsilon_Y}{\beta} \left(\frac{r_p}{r}\right)^m = \frac{\epsilon_Y}{\beta} \left(\gamma \frac{J}{\epsilon_Y \sigma_Y r}\right)^m = \frac{\epsilon_Y}{\beta} \left(\frac{K_I}{\sigma_Y}\right)^{2m} \left(\frac{\gamma}{r}\right)^m \quad (9a)$$

$$\sigma_{yy} = \sigma_{yy}(r=r_p) \left(\frac{r_p}{r}\right)^{m'} = \frac{\sigma_Y}{\beta'} \left(\frac{r_p}{r}\right)^{m'} = \frac{\sigma_Y}{\beta'} \left(\gamma \frac{J}{\epsilon_Y \sigma_Y r}\right)^{m'} = \frac{\sigma_Y}{\beta'} \left(\frac{K_I}{\sigma_Y}\right)^{2m'} \left(\frac{\gamma}{r}\right)^{m'} \quad (9b)$$

where $r_p = \gamma(K_I/\sigma_Y)^2 = \gamma J/\epsilon_Y \sigma_Y$. The values of β , β' and γ are respectively 1.41, 0.98, and 0.243 for batch C aluminum, and 1.35, 0.92, and 0.281 for batch B aluminum.

The form of Eq. (9) is similar to that given by Hutchinson^[8], and Rice and Rosengren^[9], Eq. (1). Combining Eqs. (1 and 9), with $(m+m') = 1$, one obtains

$$I_n(n)/\tilde{\sigma}_{yy}(0,n)\tilde{\epsilon}_{yy}(0,n) = \beta\beta'/\gamma \quad (10)$$

TABLE I

	N	n	β	β'	γ	$\beta\beta'/\gamma$	$I_n^{(n)}/\tilde{\sigma}_{yy}(0,n)\tilde{\epsilon}_{yy}(0,n)$
Batch B	0.22	4.5	1.35	0.92	0.28	4.4	4.4
Batch C	0.32	3.2	1.41	0.98	0.24	5.7	5.0

Table I lists the values of $(\beta\beta'/\gamma)$ obtained from the finite element calculation and the values of $(I_n/\tilde{\sigma}_{yy}\tilde{\epsilon}_{yy})$ obtained from Hutchinson's results. The values of

$\tilde{\sigma}_{yy}(0,n)$ and $\tilde{\epsilon}_{yy}(0,n)$ are obtained by the linear interpolation between $\tilde{\sigma}_{yy}(0,3) = 1.1$ and $\tilde{\sigma}_{yy}(0,13) = 1.2$; and $\tilde{\epsilon}_{yy}(0,3) = 0.7$ and $\tilde{\epsilon}_{yy}(0,13) = 0.8$; the values of $I_n(n)$ are from the linear interpolation between $I_n(3) = 3.86$ and $I_n(5) = 3.41$. The values of the finite element calculations and those obtained from Hutchinson's results are very close.

The results for σ_{yy} , ϵ_{yy} , $\bar{\sigma}$, and $\bar{\epsilon}^P$ along the radial lines of 45° , 60° , and 90° and away from the crack line are shown in Fig. 7 as solid curves. $\bar{\sigma}$ is effective stress; $\bar{\epsilon}^P$ is effective plastic strain. Similar relations can also be obtained for these stresses and strains.

The state of the crack tip stress and strain fields in SSY serves as a reference to be compared with the crack tip fields of specimens in LSY and GY.

Double-edge-notched (DEN) and single-edge-notched (SEN) specimens were studied. The calculated σ_{yy} , ϵ_{yy} , $\bar{\sigma}$, and $\bar{\epsilon}^P$ are shown in Figs. 7 and 8. For comparison, the results of the SSY calculations (solid curves) are also shown. The values of r_p for the specimens in LSY and GY are obtained by the linear extrapolation of effective stress, $\bar{\sigma}$, to yield stress σ_y in a logarithmic plot of $\bar{\sigma}$ vs r . The solid lines of the SSY coincide with the data of GY. The same scaling factor r_p is applicable to all stress and strain components. Therefore, these stresses and strains can be expressed in terms of a single parameter, r_p . Since r_p is related to K or J in SSY, these stresses and strains can also be written in terms of K or J . In other words, these stresses and strains in LSY and GY are characterized by K or J .

The fact that the data of SSY and GY fall onto the same line means that a crack tip field in GY does correspond uniquely to a crack tip field in SSY. Consequently, one will be able to use a small sample in GY to reach the crack tip field of a large sample in SSY at the equivalent K -value. The fracture process

is controlled by the crack tip stresses and strains within the stiffened zone, and the crack tip stiffened zone is imbedded within the plane stress zone. Thus, the stresses and strains within the stiffened zone will be the same if the intensity of the surrounding plane stress crack tip field is the same. Or, to state the conclusion more simply, the K or J of the plane stress crack tip field characterizes the stresses and strains within the stiffened zone, even though the stresses and strains within the stiffened zone are unknown. Therefore, if a small sample in GY fractures at a K -value so defined, a very large sample, made of the same material in SSY, will fracture at the same K -value, because the crack tip stresses and strains are identical in both samples. Since crack tip stresses and strains in the stiffened zone is affected by plate thickness, this conclusion is valid only for specimens of the same thickness.

The near tip stresses and strains correlate with K or J . In order to use the correlation for convenient fracture toughness measurements, the near tip field must be related to the applied stress σ_{∞} and the imposed elongation Δ . Fig. 9 shows the correlation of the product $\sigma_{yy} \epsilon_{yy}$ at a certain distance r ahead of a crack tip with the product $\sigma_{\infty} \Delta$ for the DEN sample. The product $\sigma_{yy} \epsilon_{yy}$ is linearly proportional to J . Therefore, we have

$$\begin{aligned} \frac{K^2}{E} &= J = 13.4 \sigma_{\infty} \Delta && \text{(batch C aluminum)} \\ \frac{K^2}{E} &= J = 13.7 \sigma_{\infty} \Delta && \text{(batch B aluminum)} \end{aligned} \tag{11}$$

These relations can be used to measure the fracture toughnesses of the DEN specimens made of these two materials.

In a cracked elastic solid, an area exists near the crack tip bounded by r_e , within which the singular terms of the characteristic crack tip stress and strain fields are valid approximations. For metallic specimens it can be shown

that if the size of $r_e \gg r_p$, K will characterize crack tip stresses and strains even with r_p [4,5]. The very existence of this conclusion serves as the basis for the empirical determination of the minimum specimen size for valid fracture toughness measurements. The condition of $r_e \gg r_p$ is known as the condition of small scale yielding. Wilson has found that the size of r_e is quite small [13] when compared with other specimen dimensions. However, r_e is linearly proportional to specimen size; so, in principle the condition of SSY can always be satisfied by using a large enough sample.

The condition of $r_e \gg r_p$ could be unduly restrictive in terms of specimen size requirements. The condition of $r_e \gg r_p$ is a sufficient condition. The necessary condition for the validity of the linear elastic fracture mechanics is that K would be able to characterize the crack tip stress or strain component at the location of the defined fracture process.

Figure 10 shows the relation between the applied stress and the equivalent K -value of a double-edge-notched specimen, both in the linear elastic fracture mechanics region and in the non-linear region. The linear elastic solution is capable to characterize the crack tip field up to $\sigma_\infty/\sigma_Y \approx 0.6$, which gives a crack line plastic zone size $r_{p(\theta=0)} \approx 0.25$ inches in comparison with the crack length $a = 0.8$ inches. In this case, the condition of $r_e \gg r_p$ is obviously more restrictive than necessary.

It can be concluded that the plane stress crack tip field of a double-edge-notched or single-edge-notched specimen in GY correlates well with the crack tip field in SSY, and that the crack tip field of a small sample in GY can be expressed in terms of K or J . The correlation is substantiated by the experimental strain measurements and the measured load-elongation curve as well as by its agreement with the analytical results of Hutchinson and Rice and Rosengren. The characteristic plane stress crack tip field is related to the product of the

applied stress and the imposed elongation. The relation can be used to measure fracture toughnesses of small samples in GY. The size of the crack tip stiffened zone is approximately equal to the plate thickness. In order to use the characteristic plane stress field, the plastic zone perhaps should be more than twice the plate thickness; i.e., $0.25 (K_c/\sigma_Y)^2 \geq 2t$. For a tough material, with $K_c = 352 \text{ MPa}\sqrt{\text{m}}$ ($320 \text{ ksi}\sqrt{\text{in}}$), $\sigma_Y = 552 \text{ MPa}$ (80 ksi), t could be up to two inches.

III. CRACK TIP OPENING DISPLACEMENT AS A FRACTURE CRITERION

When a very large crack tip plastic zone exists in a thin plate, a strip necking zone takes place, as observed by Dugdale^[6]. Plastic deformation is concentrated within the strip necking zone, and the plate thickness is greatly reduced within the strip. A strip necking zone is imbedded within a much larger plastic zone, shown schematically in Fig. 11, and a strip necking zone is shown clearly by the moire pattern in Fig. 12.

Schaeffer et. al^[14] have measured crack opening displacements as well as the relative "opening displacements" between the upper and the lower boundaries of the strip necking zone. Their measurements agree very well with the calculated values according to the Dugdale strip yielding model. The length of the strip necking zone has to be several times the thickness of the plate in order to assure a good agreement. The length of the strip necking zone, relative to plate thickness, t , is given by the parameter $\eta = (K/\sigma_Y)^2/t$. For the specimens tested by Schaeffer et al, $\eta = 48$. Furthermore, they have found that the opening displacements within the strip necking zone equal the thickness contraction.

As K increases, and a crack grows slowly toward a point ahead of the crack tip, the relative opening displacement at the point in the strip necking zone increases while the thickness is reduced. Once the crack tip passes the point, the plate thickness at the point stops changing. After a specimen is broken, the thickness at a point along the fracture path is the same thickness, when the crack

tip first reached the point. The thickness contraction, Δt , at the point equals the crack tip opening displacement, CTOD, and CTOD is directly related to the applied K . According to the Dugdale model^[15],

$$CTOD = K^2 / E\sigma_y \quad (12)$$

for small scale yielding. Therefore the K -values during stable crack growth can be obtained by plate thickness measurements along the fracture surface of a broken specimen. Indeed, Liu and Kuo^[16] have measured the fracture resistance curve as well as K_c from thickness measurements in such a manner. The thickness contraction fracture toughness measurements can be used economically for screening tests.

When strip necking takes place, CTOD is the result of the stretch of the materials within the strip necking zone. In this case, the crack tip opening displacement is a "tangible" physical quantity, that can be measured directly.

Experimental observations showed that crack tip necking began to form at η equal to about 18^[17]. For specimens in which η is between 18 and 48, the strip necking zone is not large enough to warrant the use of the thickness contraction as a fracture toughness measurement.

Using the moire method^[17,18], COD were measured in specimens made of 2024-0, 2024-T3, and 2024-T351 aluminum alloys with tensile yield strengths, 54, 310, and 383 MN/m², respectively. All specimens were 101.6 mm wide central crack panels with a nominal crack length of 17.8 mm. The applied stresses were about one half the yield strengths for all of the specimens. The density of the moire grille is 528 lines/mm, and is capable of measuring COD of about 2.5×10^{-4} mm (10^{-5} in), using the rotational mismatch technique^[19]. Figure 13 shows the measured COD. The dashed lines are calculated from the Dugdale model and the solid lines from the elastic model. Figure 13a shows two specimens at the same K -value. Specimen 1 is much thinner than specimen 2. The thinner specimen ($\eta = 1.75$) agrees very

well with the Dugdale model, and the thicker one ($\eta = 1.12$) agrees with the elastic model. Approaching the crack tip, the difference in COD is more than a factor of two. It is not likely that the crack tip opening displacement of specimen 2 will be equal to that given by the Dugdale model. Similar data is shown in Fig. 13b. It can be concluded that when η is close to 18, the measured COD's agree exceedingly well with the Dugdale model. When η is close to one or less, the measured COD's agree well with the elastic calculations. When the COD measurements agree with the Dugdale model, the measured COD can be used to infer a CTOD according to the Dugdale model and the inferred CTOD relates to K by Eq. (12). The inferred CTOD characterizes crack tip deformation and crack tip stresses. Therefore it is a suitable choice as a fracture criterion. It should be emphasized that no strip necking zone was observed in the thin specimens despite the fact that the COD's in these specimens agreed well with the Dugdale model, which assumes a strip yield zone.

The agreement in COD between the measurements and the Dugdale model was observed for aluminum specimens in small scale yielding or prior to general yielding. Figure 14 shows the COD measurements in a magnesium specimen by Kobayashi et al.^[20]. All curves are beyond general yielding. The points shown in the figure were calculated in this investigation with the Dugdale model for curve Mg-1-1Y, which was at the incipience of general yielding. The measurements agree well with the Dugdale model even in the general yielding condition. The agreement of the measured and the calculated COD both in SSY and in GY supports the Dugdale model for fracture toughness measurements. Figure 14 also shows that crack opening profiles are parallel once beyond general yielding. When the upper and the lower crack surfaces move apart like two rigid surface, the area ahead of the crack tip is stretched, and the added stretch gives more opening displacement at the crack

tip. During the process of crack tip opening stretching, the crack profile maintains its original shape, corresponding to that at the incipience of general yielding. Let $\delta\text{COD}(r)$ be the difference of the crack opening displacement at r , $\text{COD}(r)$, and the crack tip opening displacement at the incipience of general yielding. Once beyond general yielding, the $\delta\text{COD}(r)$ remains unchanged. The total $\text{COD}(r)$ beyond general yielding is the sum of $\delta\text{COD}(r)$ and CTOD , i.e.,

$$\text{COD}(r) = \delta\text{COD}(r) + \text{CTOD}$$

or

(13)

$$\text{CTOD} = \text{COD}(r) - \delta\text{COD}(r)$$

$\delta\text{COD}(r)$ can be calculated by the finite element method. CTOD can be obtained from the measured $\text{COD}(r)$ and the calculated $\delta\text{COD}(r)$. CTOD is related to K by Eq. (12).

Equation (13) is applicable to center cracked panels. For the compact tension specimens, an additional term should be added to account for the rigid body rotation about a "plastic-hinge". The rotational effects remain to be investigated.

The finite element method, based on the Dugdale model, can be used to calculate $\delta\text{COD}(r)$ for plates of arbitrary shape. Hayes and William^[21] have used the finite element method to calculate COD and CTOD for the central crack, double-edge crack, single-edge crack, and circumferential crack specimens under various load levels up to general yielding. Basically, Hayes and Williams's method balances the stress intensity factors contributed from the remote applied stress and the stresses in the strip yielding zone.

Equation (12) has been indiscriminantly used to relate CTOD to K without the consideration of the thickness effect. The equation is applicable when $\eta \geq 18$. For specimens of lower η -values, Eq. (12) needs to be modified by a parameter which is thickness dependent.

There exist several methods to measure CTOD, such as the load-line mouth opening and plastic hinge method, the linear extrapolation of a crack opening profile from an optical photograph, rubber infiltration, etc. None of these methods can avoid some degree of arbitrariness, either in the relation between the far field measurement and the near tip deformation behavior or in the relation between the measured quantity and the inferred K-value. Perhaps some of the earlier difficulties in applying CTOD to fracture toughness measurements arise from such arbitrariness. The method and the procedure outlined in this study will help to avoid these difficulties.

IV. SUMMARY AND CONCLUSIONS

1. The stresses and strains in a cracked solid are in a complicated 3-dimensional state. There are three 2-dimensional limiting cases: plane strain, plane stress, and the Dugdale strip yielding case. The parameter $\eta = (K/\sigma_Y)^2/t$ determines which one of these three limiting cases is predominant. The characteristic crack tip fields of these three cases differ vastly.
2. Fracture process is controlled by the stresses and strains at the crack tip. Because of the difference in the characteristics of the crack tip field, there exist various regimes of fracture correlations between a small laboratory sample in general yielding and a large engineering structure in small scale yielding.
3. Crack tip strip necking has been observed, when η is 48. At $\eta = 48$, the measured relative opening displacements between the upper and the lower boundaries of the strip necking zone, including that at the crack tip, agree well with the calculated values according to the Dugdale strip yielding model. Furthermore the relative opening displacement in the strip necking zone is equal to the thickness contraction. According to the Dugdale model,

$$K = (E\sigma_Y \text{ CTOD})^{1/2} = (E\sigma_Y \Delta t)^{1/2}$$

where Δt is thickness contraction.

4. When η is 18, crack tip necking zone begins to form, and the measured crack opening displacements agree extremely well with the calculations based on the Dugdale strip yielding model. Once general yielding is reached, the upper and the lower crack surfaces move apart as two rigid surfaces. The difference between the crack opening displacement at a distance r , $COD(r)$, and crack tip opening displacement, CTOD, remains unchanged once beyond general yielding.

$$\delta COD(r) = COD(r) - CTOD$$

$\delta COD(r)$ can be calculated by the finite element method. CTOD can be obtained from the calculated $\delta COD(r)$ and the measured $COD(r)$; and CTOD is related to K . Thus for η between 18 and 48, we have

$$\begin{aligned} K &= (E\sigma_Y CTOD)^{1/2} \\ &= \{E\sigma_Y [COD(r) - \delta COD(r)]\}^{1/2} . \end{aligned}$$

5. When r_p is several times larger than the plate thickness but it is not large enough to form the crack tip necking zone, a characteristic plane stress crack tip field exists. For double-edge-notched and single-edge-notched samples, there is a unique correspondence between the crack tip field in a small sample in general yielding and the crack tip field in a very large sample in small scale yielding. Therefore the equivalent K -value of such a small sample can be established. Furthermore, the near tip stresses and strains are related to the applied stress and the imposed elongation. Therefore the fracture toughnesses of such small samples can be measured conveniently for η between 10 and 18.

In summary, as shown in Fig. 15, when η is more than 48, thickness contraction can be used to measure K ; when η is between 18 and 48, the COD can be used to measure equivalent K ; and when η is between 10 and 18, the correspondence between the crack tip fields in small scale yielding and in general yielding can be used to measure the fracture toughness of a ductile and tough material. However, the demarcations between the various regions are tentative. Additional studies are needed to establish them firmly.

ACKNOWLEDGMENT

The authors are indebted to Mr. Robert Heyer for his sustained support during the initial period of the research program and for his farsightedness in recognizing the importance of plastic deformation to the development of the non-linear fracture mechanics. The authors also wish to acknowledge the financial supports by American Iron and Steel Institute (Contract No. 123) and Army Research Office (Contract No. DAAG-78-G0069) and the assistance in manuscript preparation by Mrs. H. Turner and Mr. R. Ziemer.

References

- [1] Griffith, A. A., "The Phenomena of Rapture and Flow in Solids," Philosophical Transactions of the Royal Society (London) Series A, Vol. 221, 1921, pp. 163-198.
- [2] Irwin, G. R., "Fracture Dynamics," Fracturing of Metals, Am. Society for Metals (Cleveland) 1948, pp. 147-166.
- [3] Orowan, E., "Energy Criteria of Fracture," Welding Research Equipment, Vol. 20, 1955, p. 1575.
- [4] Liu, H. W., "Discussion to 'A Critical Appraisal of Fracture Mechanics'," 1965, pp. 23-26.
- [5] Liu, H. W., "Fracture Criteria of Cracked Metallic Plate," International Journal of Fracture Mechanics, Vol. 2, 1966, pp. 393-399.
- [6] Dugdale, D. S., "Yielding of Steel Sheets Containing Slits," Journal of Mech. and Phys. of Solids, Vol. 8, 1960, pp. 100-104.
- [7] Gavigan, W. J., Liu, H. W. and Ke, J. S., "Local and Gross Deformation in Cracked Metallic Plates and an Engineering Ductile Fracture Analysis," ASME Paper 71-PVP-52, 1971.
- [8] Hutchinson, J. W., "Singular Behavior at the End of a Tensile Crack in a Hardening Material," Journal of Mech. and Phys. of Solids, Vol. 16, 1968, p. 13.
Hutchinson, J. W., Nonlinear Fracture Mechanics, Technical University of Denmark, 1979.
- [9] Rice, J. R. and Rosengren, G. F., "Plane Strain Deformation Near a Crack Tip in a Power-Law Hardening Material," Jour. of Mech. and Phys. of Solids, Vol. 16, 1968, p. 1.
- [10] Hu, W. L. and Liu, H. W., "Crack Tip Strain - A Comparison of FEM Calculations and Measurements," Proceedings of the Ninth National Symposium of Fracture Mechanics, Pittsburgh, Pa., August 1975, ASTM STP 601, Crack and Fracture, 1976.
- [11] Hancock, J. W. and Cowling, M. J., "Role of State of Stress in Crack-tip Failure Processes," Metal Science, Aug.-Sept. 1980, pp. 293-304.
- [12] Hu, W. L., "A Finite Element Study on Crack Tip Deformation," Ph.D. Dissertation, Solid State Science and Technology, Syracuse University, 1976.
- [13] Wilson, W. K., Discussion on "Plane Strain Crack Toughness Testing," ASTM STP 410, 1969, p. 75.
- [14] Schaeffer, B. J., Liu, H. W. and Ke, J. S., "Deformation and the Strip Necking Zone in a Cracked Steel Sheet," Experimental Mech., April, 1971, pp. 172-175.

- [15] Rice, J. R., "Mechanics of Crack Tip Deformation and Extension by Fatigue," ASTM STP 415, Fatigue Crack Propagation, 1967, pp. 247-309.
- [16] Liu, H. W. and Kuo, A. S., "Fracture Toughness of Thin and Tough Plates," International Journal of Fracture, 14, 1978, pp. R-109-R112.
- [17] Kuo, A. S. and Liu, H. W., "An Experimental and FEM Study on Crack Opening Displacement," Proceedings of the 23rd Sagamore Army Material Research Conference, Plenum Press., N. Y., 1979, pp. 385-408.
- [18] Kuo, A. S., "An Experimental and FEM Study on Crack Opening Displacement and Its Application to Fatigue Crack Growth," Ph.D. Dissertation, Solid State Science and Technology, Syracuse University, 1976.
- [19] Kuo, A. S. and Liu, H. W., "Moir Method - Its Potential Application to NDT," in Nondestructive Evaluation of Materials, Proceedings 23rd Sagamore Army Material Research Conference, Plenum Press, N.Y., 1979, pp. 385-408.
- [20] Kobayashi, A. S., Engstrom, W. L. and Simon, B. R., "Crack Opening Displacements and Normal Strains in Centrally Notched Plates," Experimental Mechanics, April 1969, pp. 163-170.
- [21] Hayes, D. J. and Williams, J. G., "A Practical Method for Determining Dugdale Model Solutions for Cracked Bodies of Arbitrary Shape," International Journ.of Frac. Mech., Vol. 8, No. 3, Sept. 1972, pp. 239-256.

FIGURE CAPTIONS

FIGURE 1. COMPARISON OF CALCULATED ϵ_{yy} VERSUS EXPERIMENTAL MEASUREMENTS, DOUBLE-EDGE-NOTCHED PLATE, 2024-0 ALUMINUM ALLOY. Δ = ELONGATION OF GAGE LENGTH, GL. $E = 6.9 \times 10^4$ MPa (10^4 ksi).

Batch	σ_y		N	W		a		GL	
	MPa	ksi		mm	Inches	mm	Inches	mm	Inches
A	47.6	6.9	0.31	104	4.1	19.4	0.764	168	6.625
B	69	10	0.22	208	8	40.6	1.6	356	14.0
C	50	7.26	0.315	102	4	20.3	0.8	178	7.0

FIGURE 2. THE MEASURED AND CALCULATED LOAD-ELONGATION CURVES
A = AREA, W = WIDTH.

FIGURE 3. SCHEMATIC PLOT OF STRESS AND STRAIN DISTRIBUTIONS AHEAD OF A CRACK IN LOGARITHMIC SCALE.

FIGURE 4. SLIP LINE FIELDS FOR FULLY PLASTIC TENSION MODE . PLANE STRAIN.

FIGURE 5. ELEMENT LAYOUT FOR SMALL SCALE YIELDING CALCULATIONS.

FIGURE 6. NORMALIZED PLOTS OF CRACK LINE STRESSES AND STRAINS.

FIGURE 7. CORRELATIONS OF σ_{yy} , ϵ_{yy} , $\bar{\sigma}$, and $\bar{\epsilon}^p$ BETWEEN THE SMALL SCALE YIELDING AND DOUBLE-EDGE-NOTCHED SPECIMEN LOADED INTO THE REGION OF GENERAL YIELDING.

FIGURE 8. CORRELATIONS OF σ_{yy} , ϵ_{yy} , $\bar{\sigma}$ AND $\bar{\epsilon}^p$ BETWEEN THE SMALL SCALE YIELDING AND SINGLE-EDGE-NOTCHED SPECIMEN LOADED INTO THE REGION OF GENERAL YIELDING.

FIGURE 9. NEAR FIELD PARAMETER, $\sigma_{yy}\epsilon_{yy}$ VERSUS FAR FIELD PARAMETER, $\sigma_{\infty}\Delta$

FIGURE 10. CALCULATED STRESS INTENSITY FACTOR AT VARIOUS LOADING LEVELS.

FIGURE 11. CHEMATIC DIAGRAM OF CRACK TIP NECKING.

FIGURE 12. MOIRE PATTERN OF A STEEL SPECIMEN: APPLIED STRESS 55 ksi; 0.2%
OFFSET YIELD STRESS 91 ksi; YOUNG'S MODULUS 32×10^6 psi; 0.012
INCHES THICK; 6 INCHES WIDE; SLOT LENGTH 1 INCH; PITCH OF MOIRE
GRILLE 1/13,400 INCHES.

FIGURE 13. THICKNESS EFFECTS ON COD. DASHED LINE - DUGDALE MODEL. SOLID LINE - ELASTIC MO

FIGURE 14. COD IN MAGNESIUM [From A. S. Kobayashi et. al, Ref. 20].

FIGURE 15. THICKNESS EFFECTS ON THE CHOICE OF FRACTURE CRITERIA.

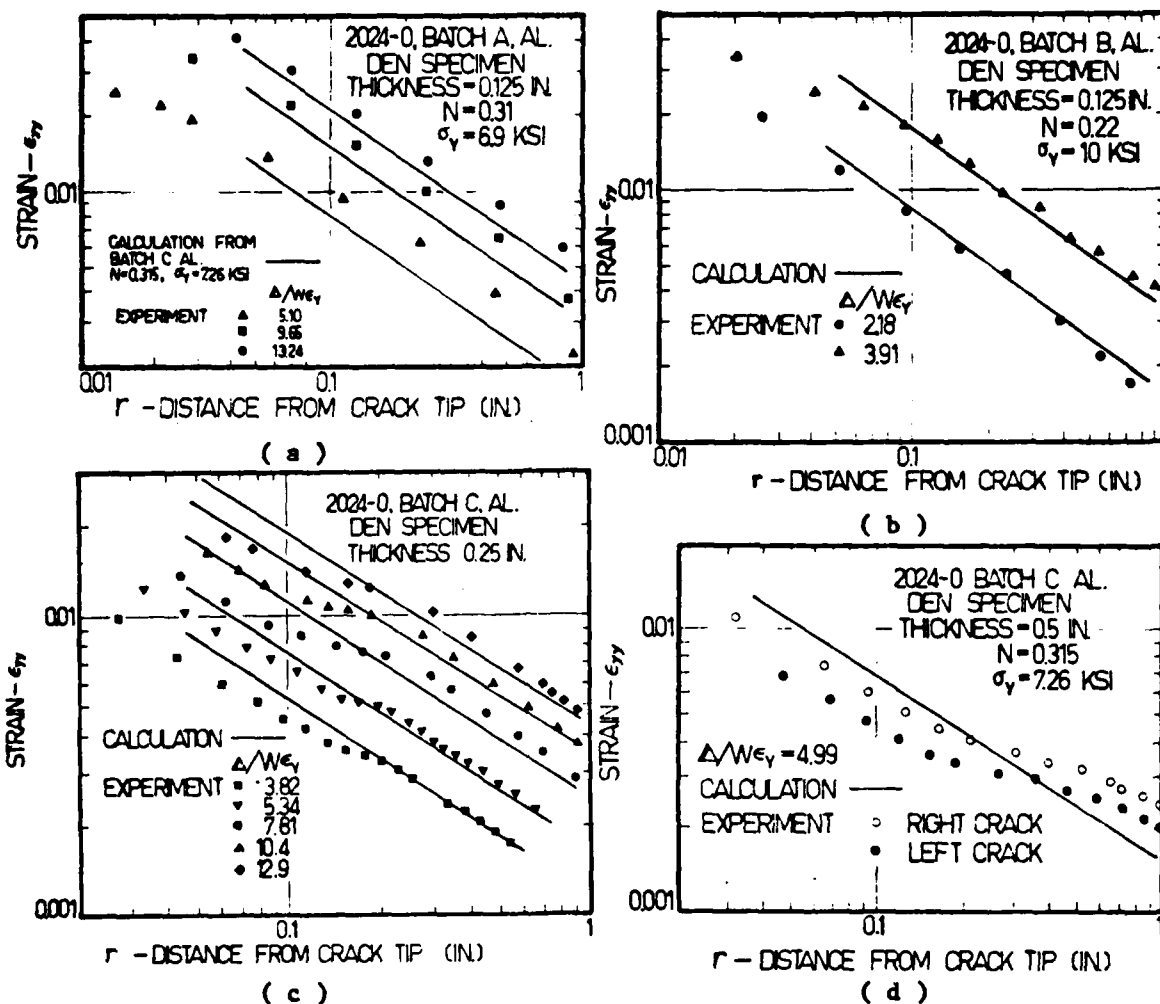


FIGURE 1. COMPARISON OF CALCULATED ϵ_{yy} VERSUS EXPERIMENTAL MEASUREMENTS, DOUBLE-EDGE-NOTCHED PLATE, 2024-O ALUMINUM ALLOY. Δ = ELONGATION OF GAGE LENGTH, GL.
 $E = 6.9 \times 10^4 \text{ MPa } (10^4 \text{ ksi})$.

	σ_y		N	W		a		GL	
Batch	MPa	ksi		mm	Inches	mm	Inches	mm	Inches
A	47.6	6.9	0.31	104	4.1	19.4	0.764	168	6.625
B	69	10	0.22	208	8	40.6	1.6	356	14.0
C	50	7.26	0.315	102	4	20.3	0.8	178	7.0

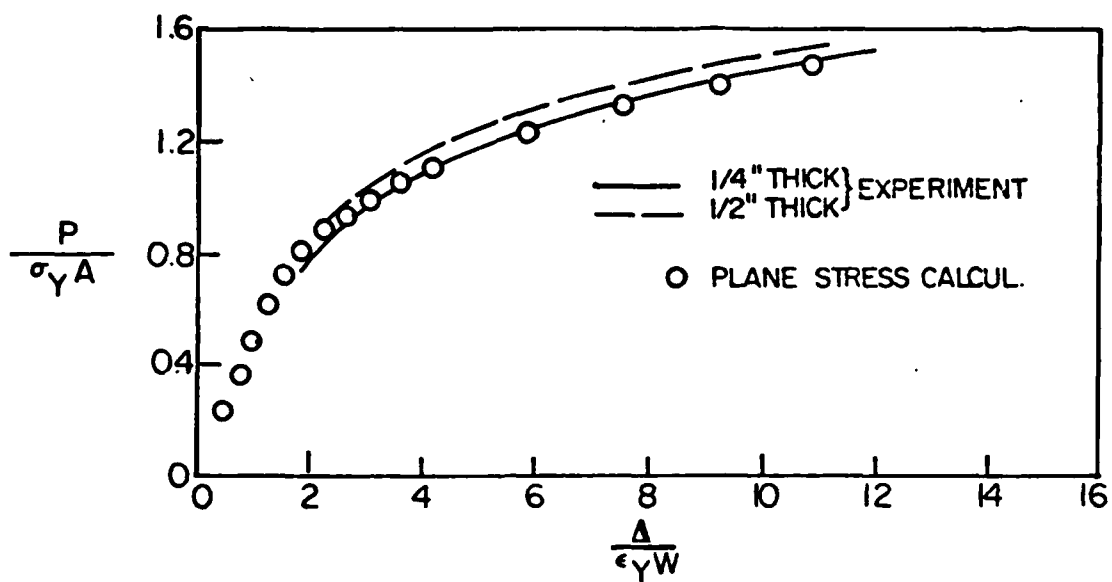


FIGURE 2. THE MEASURED AND CALCULATED LOAD-ELONGATION CURVES
A = AREA, W = WIDTH.

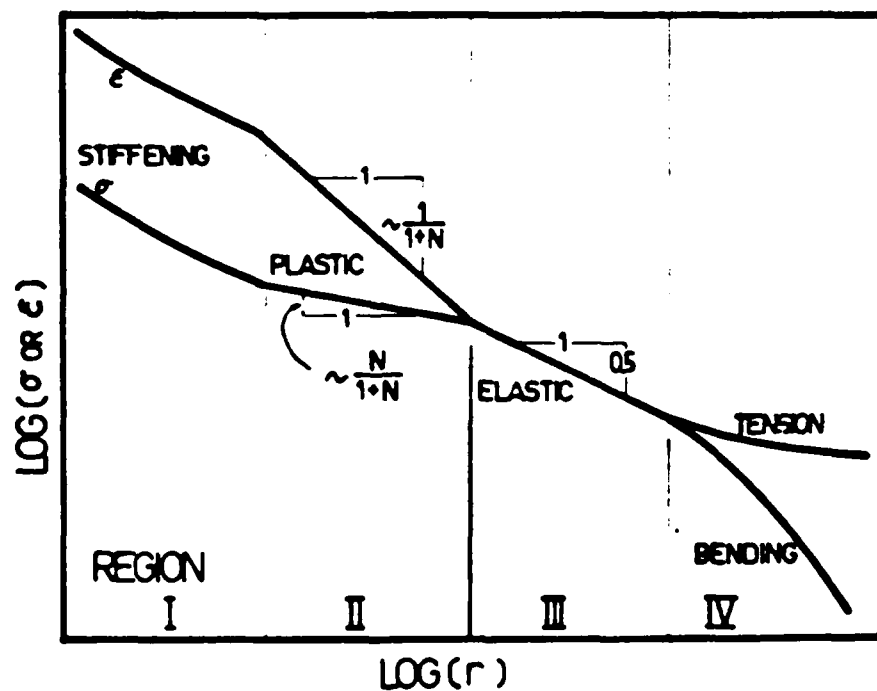


FIGURE 3. SCHEMATIC PLOT OF STRESS AND STRAIN DISTRIBUTIONS AHEAD OF A CRACK
IN LOGARITHMIC SCALE.

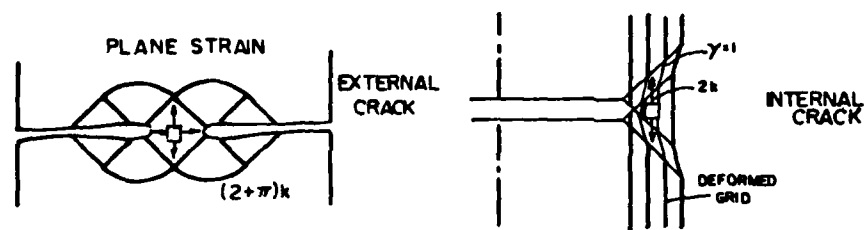


FIGURE 4. SLIP LINE FIELDS FOR FULLY PLASTIC TENSION MODE . PLANE STRAIN.

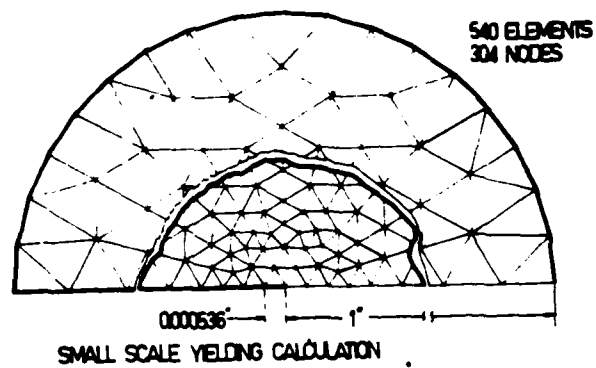


FIGURE 5. ELEMENT LAYOUT FOR SMALL SCALE YIELDING CALCULATIONS.

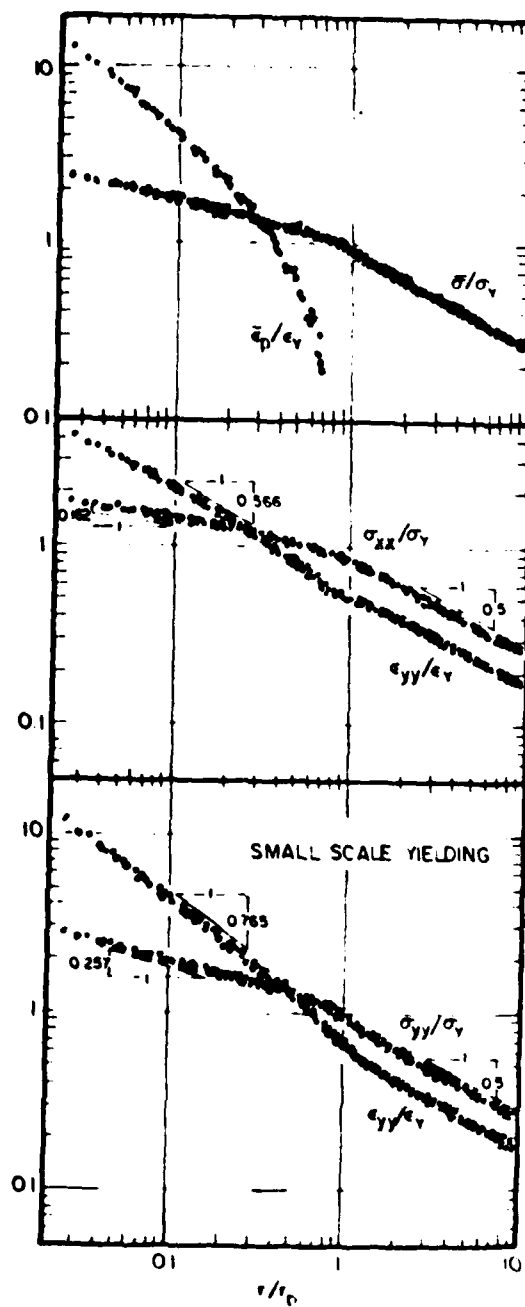


FIGURE 6. NORMALIZED PLOTS OF CRACK LINE STRESSES AND STRAINS.

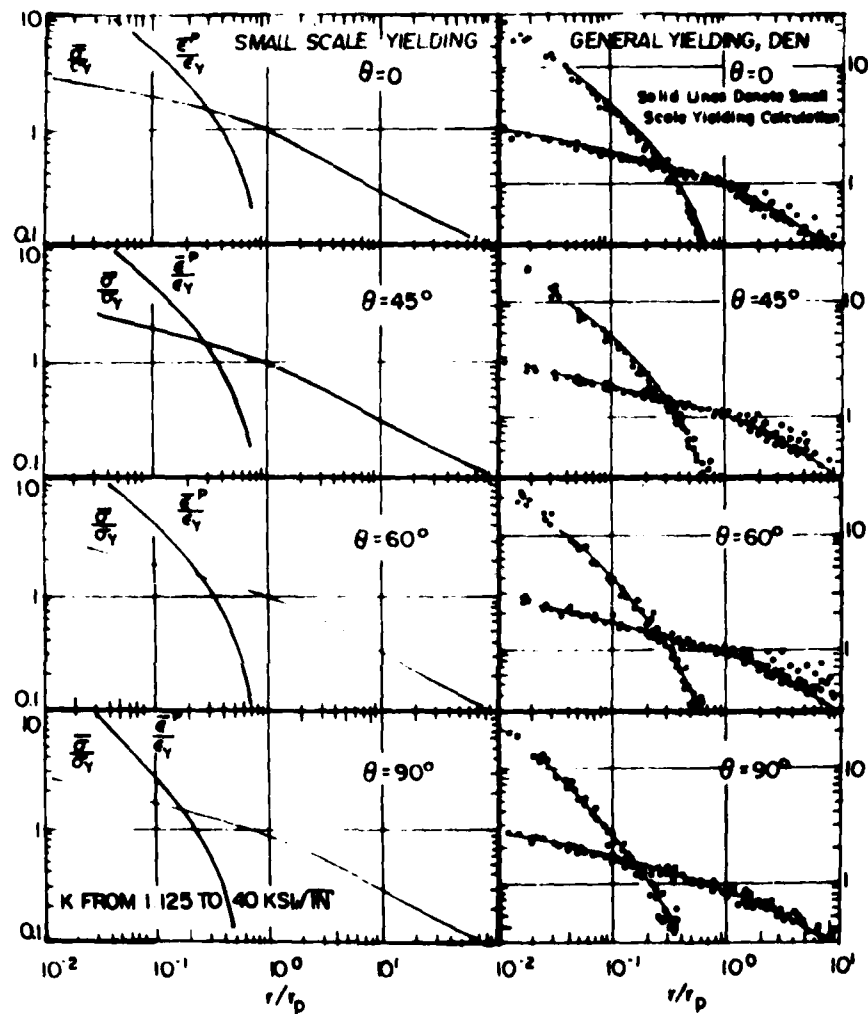


FIGURE 7a. CORRELATIONS OF $\bar{\sigma}$ AND $\bar{\epsilon}^D$ BETWEEN THE SMALL SCALE YIELDING AND DOUBLE-EDGE-NOTCHED SPECIMEN LOADED IN GENERAL YIELDING.

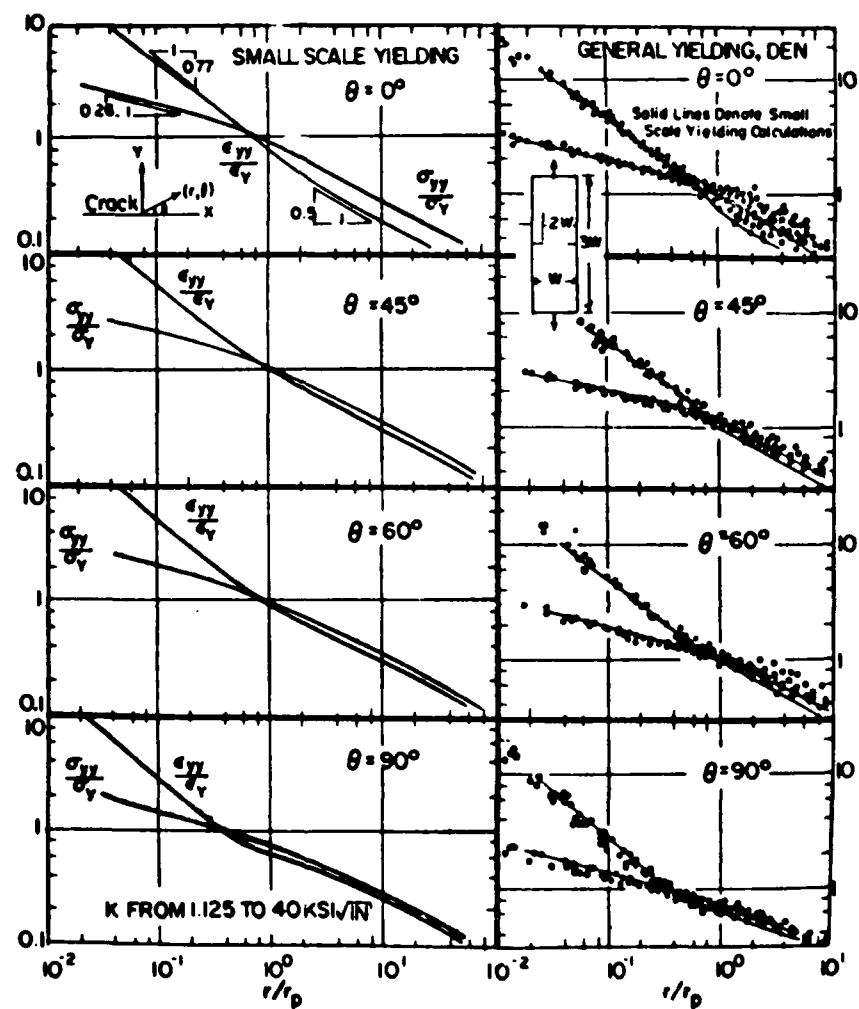


FIGURE 7b. CORRELATIONS OF σ_{yy} AND ϵ_{yy} BETWEEN THE SMALL SCALE YIELDING AND DOUBLE-EDGE-NOTCHED SPECIMEN LOADED IN GENERAL YIELDING.

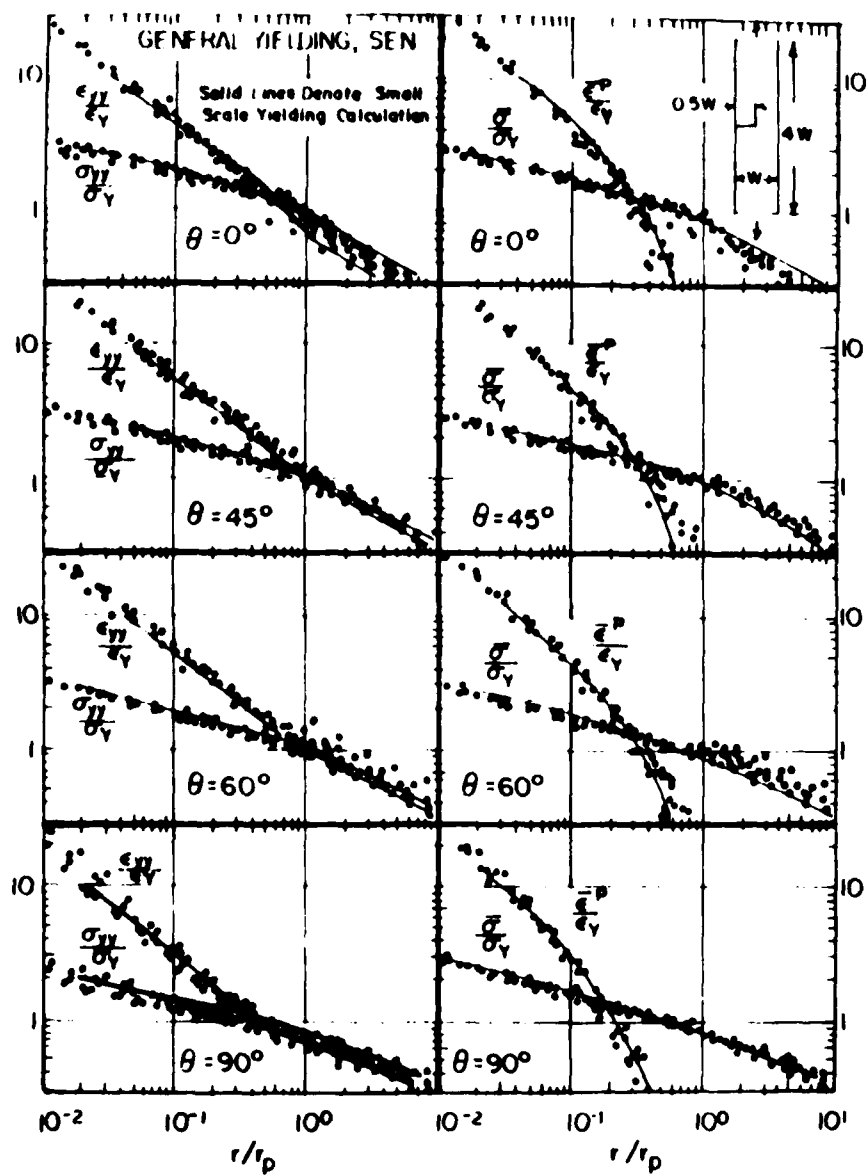


FIGURE 8. CORRELATIONS OF σ_{yy} , ϵ_{yy} , $\bar{\epsilon}$ AND $\bar{\epsilon}^p$ BETWEEN THE SMALL SCALE YIELDING AND SINGLE-EDGE-NOTCHED SPECIMEN LOADED INTO THE REGION OF GENERAL YIELDING

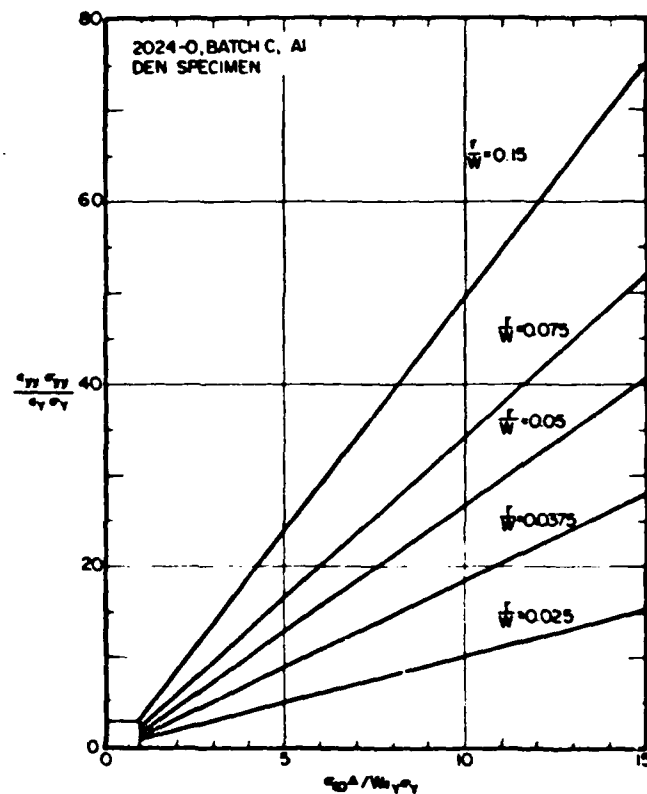
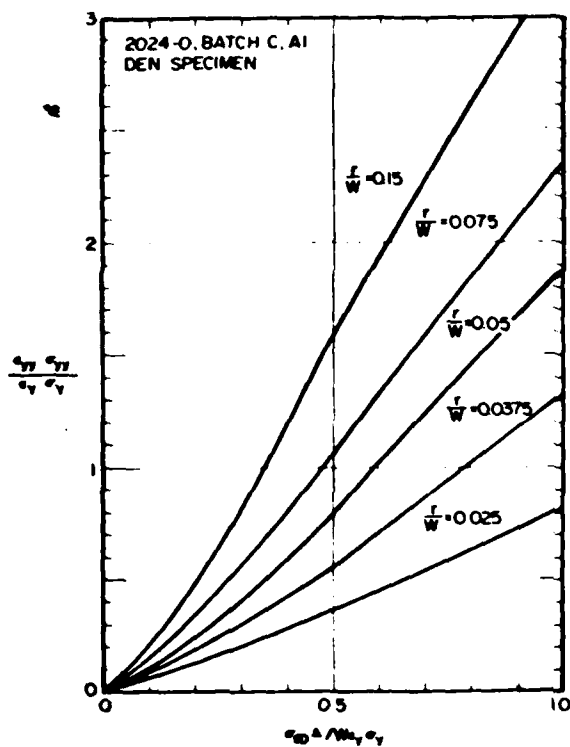


FIGURE 9. NEAR FIELD PARAMETER, $\sigma_{yy} \epsilon_{yy}$ VERSUS FAR FIELD PARAMETER, $\sigma_{xx} \Delta$

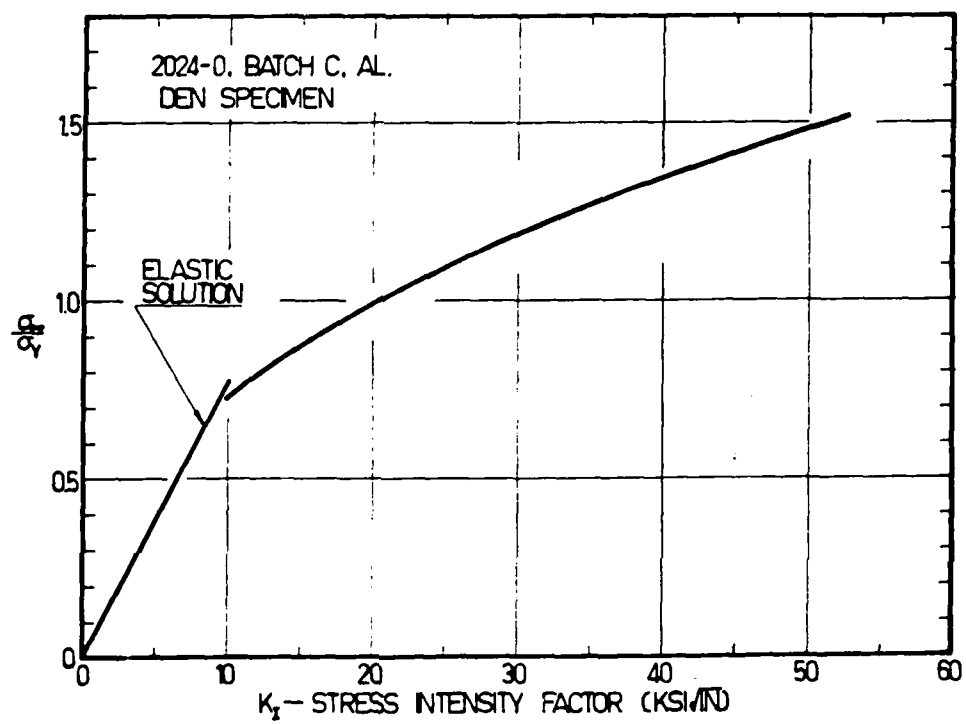


FIGURE 10. CALCULATED STRESS INTENSITY FACTOR AT VARIOUS LOADING LEVELS.

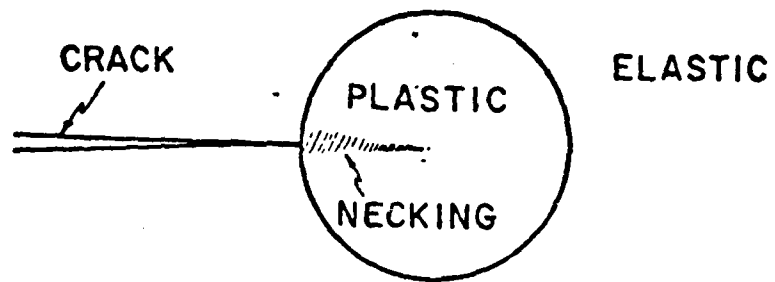


FIGURE 11. SCHEMATIC DIAGRAM OF CRACK TIP NECKING.

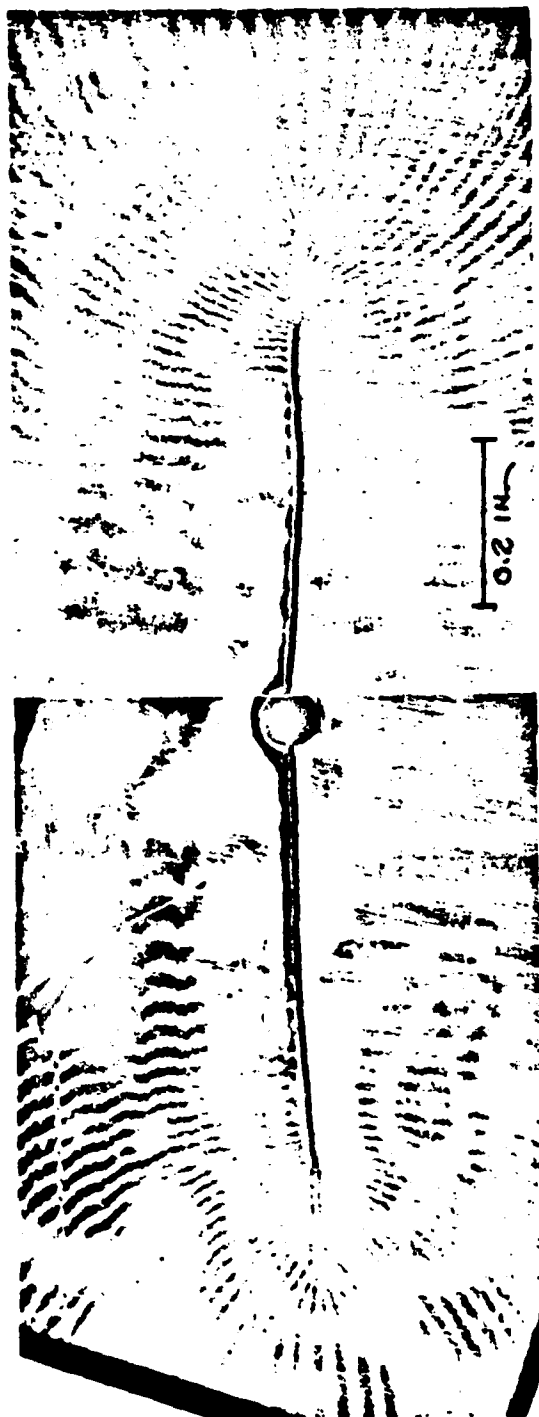
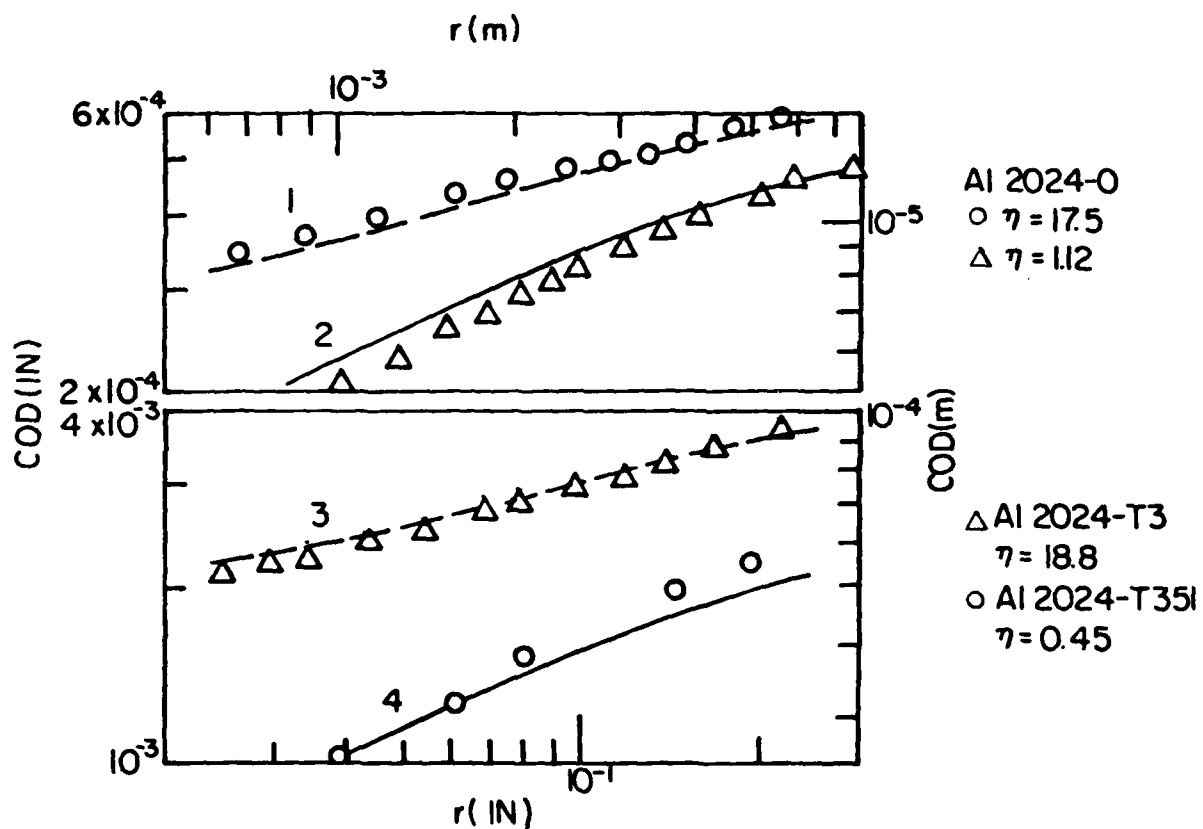


FIGURE 12 MOIRE PATTERN OF A STEEL SPECIMEN: APPLIED STRESS 55 KSI; 0.2% OFFSET YIELD STRESS 91 KSI; YOUNG'S MODULUS 32×10^6 PSI; 0.012 INCHES THICK; 6 INCHES WIDE; SLOT LENGTH 1 INCH; PITCH OF MOIRE GRILLE $1/13,400$ INCHES, $K, 69.6 \text{ KSI } \sqrt{\text{IN}}$



Spec. No.	Material	σ_Y MN/m ²	K MN/m ^{3/2}	t mm	η (K/ σ_Y) ² /t	COD Model
1	Al 2024-O	54	4.53	0.41	17.5	Dugdale
2	Al 2024-O	54	4.53	6.25	1.12	Elastic
3	Al 2024-T3	310	28.2	0.38	18.8	Dugdale
4	Al 2024-T351	386	20.4	6.25	0.45	Elastic

FIGURE 13. THICKNESS EFFECTS ON COD.

Dashed line - Dugdale model.
Solid line - Elastic model.

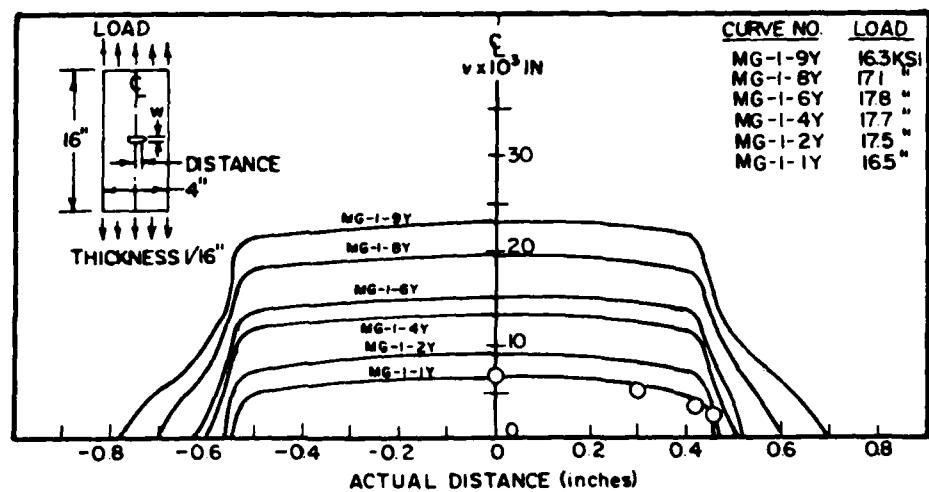


FIGURE 14. COD IN MAGNESIUM [From A. S. Kobayashi et. al, Ref. 20].

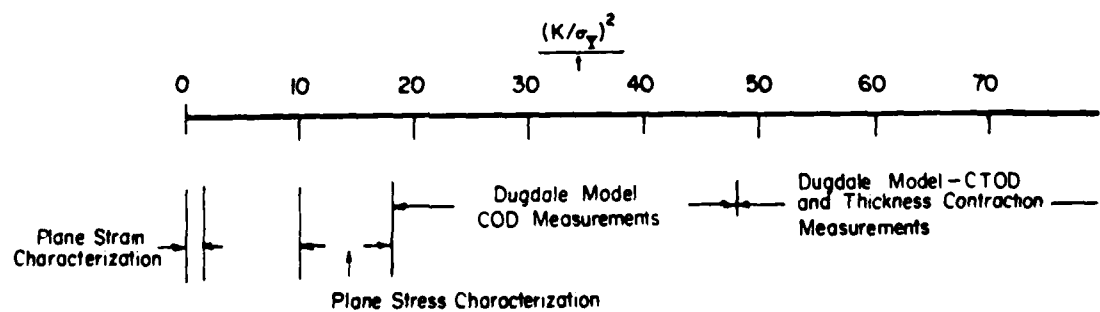


FIGURE 15. THICKNESS EFFECTS ON THE CHOICE OF FRACTURE CRITERIA.

APPENDIX II

CRACK TIP DEFORMATION AND FATIGUE CRACK GROWTH

H. W. Liu

Professor of Materials Science

Presented at the

ASME Symposium on "Mechanics of Fatigue"
Washington, D.C.

November 16, 1981

TO BE PUBLISHED
IN THE PROCEEDINGS

Department of Chemical Engineering and Materials Science
SYRACUSE UNIVERSITY
Syracuse, New York 13210

ABSTRACT

Fatigue crack growth is caused by crack tip cyclic plastic deformation. Both the macro-analysis and the moiré strain measurements indicate that crack tip cyclic deformation is a function of ΔK , R-ratio, and plate thickness, t . Therefore, da/dN must be dependent on these three parameters.

The cyclic crack tip unzipping shear decohesion process is described, and the unzipping fatigue crack growth process is modelled by the finite element method. The calculated crack growth rate agrees well with the experimental measurements. The unzipping model is used to study the growth of micro-cracks and the fatigue crack growth in a ferritic-martensitic two phase steel.

A model of fatigue crack growth threshold is proposed. The proposed model agrees with the observed crack growth behavior in the near threshold region. A quantitative analysis of fatigue limit and microstructure is made. The analysis provides a quantitative approach to optimize the microstructure for high fatigue strength.

INTRODUCTION

Plastic deformation in crystalline materials takes place in discrete parallel planes separated by crystal layers which are practically "deformation free" [1]. This deformation process may occur at a crack tip and cause a crack to grow under cyclic loading.

The use of a single parameter ΔK to characterize crack tip cyclic plastic deformation has been analyzed [2,3]. Moiré strain measurements [4] showed that ΔK does characterize both the cyclic strain range and the total accumulated strain in the crack tip region. The capability of ΔK to characterize crack tip deformation is the basis for the use of ΔK to correlate fatigue crack growth rate. The analysis and the moiré strain measurements are reviewed briefly.

Alternating shear at two intersecting conjugate slip planes, crack tip blunting, and shear decohesion have been proposed as the mechanisms for fatigue crack growth [5,6,7,8]. The unzipping model of fatigue crack growth based on crack tip shear decohesion process was modelled by the finite element method [9].

The calculated crack growth rate compares favorably with crack growth rate and striation spacing measurements. The unzipping model was extended to study the growth of micro-cracks and the fatigue crack growth in a ferritic-martensitic two phase steel [10,11].

-2-

When the applied ΔK is low enough, a crack stops propagating. ΔK_{th} is the ΔK for crack growth threshold. Based on the unzipping shear decohesion process, a model for ΔK_{th} is proposed. The proposed model agrees with the crack growth behavior in the near threshold region.

A quantitative analysis on the fatigue limit of a two-phase ferritic-martensitic steel is made. The fatigue limit of such steel could be controlled by the crack non-nucleation or crack non-propagation in the ferrite or in the martensite; the fatigue limit could be controlled by the constraint of the hard martensite on the crack tip deformation in the ferrite; it can also be controlled by the cracking resistance of the martensite. The relation between the dominant controlling process and the ferrite domain size is analyzed.

CRACK TIP DEFORMATION - ΔK CHARACTERIZATION [2,3]

During the last twenty years, linear elastic fracture mechanics has been applied extensively to fatigue crack growth. Linear elastic fracture mechanics is based on the characteristic crack tip stress field in a linear elastic solid. The elastic stresses, strains, and displacements for a Mode I crack are

$$\begin{aligned}\sigma_{ij} &= \frac{K_I}{\sqrt{2\pi r}} \tilde{\sigma}_{ij}(\theta) \\ \epsilon_{ij} &= \frac{K_I}{2\mu\sqrt{2\pi r}} \tilde{\epsilon}_{ij}(\theta, \nu) \\ u_i &= \frac{K_I}{2\mu} \sqrt{\frac{r}{2\pi}} \tilde{u}_i(\theta, \nu)\end{aligned}\tag{1}$$

where r, θ are polar coordinates; and $\tilde{\sigma}_{ij}, \tilde{\epsilon}_{ij}, \tilde{u}_i$ prescribe the distributions of the corresponding $\sigma_{ij}, \epsilon_{ij}$, and u_i components. K_I is the stress intensity factor while ν is Poisson's ratio.

These relations are valid only in a region very close to a crack tip, and we call this region the characteristic elastic crack field zone, r_e . Outside this region, the approximations of these relations deteriorate rapidly. Within r_e , the stresses increase rapidly as r approaches the tip. The high stresses cause plastic deformation within a small region close to the tip in a metallic specimen. The plastic region is defined by $r_p(\theta)$.

Figure 1 shows two samples that have different geometry and forms of loading. However, these two samples are loaded to the same K -value. Without plastic deformation, the elastic stresses within r_e 's of these two samples are the same. With plastic deformation, if $r_p \ll r_e$, the stresses on the outer boundaries of r_e 's are not perturbed much by the stress relaxation within r_p 's, and the stresses on the boundaries of these two r_e 's are essentially given by the elastic solution.

Figure 2 shows the two regions of r_e 's as free bodies of the same shape and size. If the condition of $r_p \ll r_e$ is satisfied, their boundary stresses must be the same since $K_1 = K_2$. Therefore, the stresses and strains at the same point $P(r, \theta)$ in these two free bodies also must be the same. Furthermore, if the same cyclic loading (in terms of K), are applied to these two samples, the fluctuations of the boundary stresses on these two free bodies are the same, and the cyclic stresses and strains at the same point $P(r, \theta)$ within these two regions of

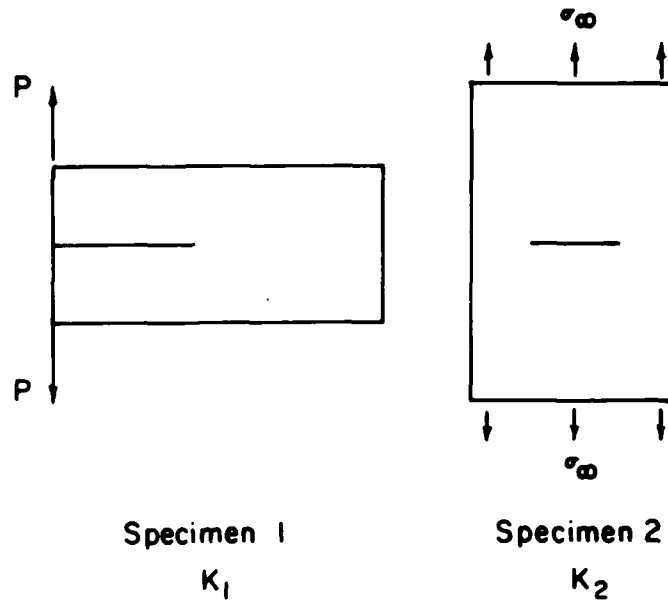


Fig. 1. Two different specimen geometry, two different forms of loading, but $K_1 = K_2$.

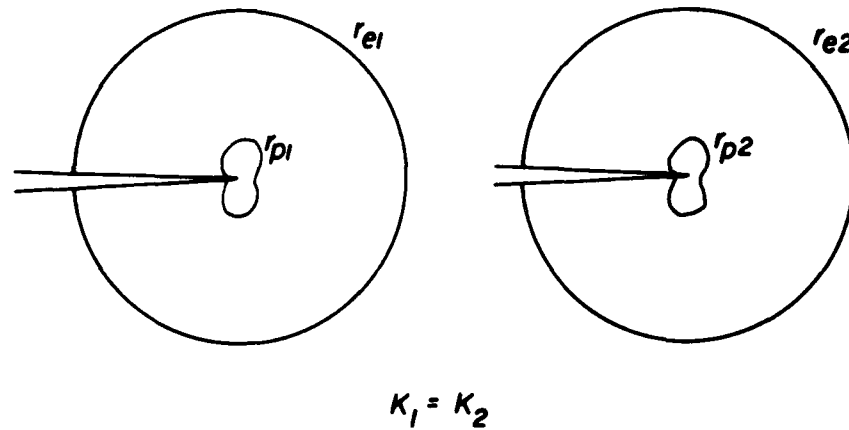


Fig. 2. Two free bodies of same shape and size. With same boundary stresses.

r_e must be the same even within r_p . If the same fluctuation of K is applied to these two samples (provided the ratio r_p/a is not excessively large), the cyclic stresses and strains experienced by these two material points at $P(r, \theta)$ are the same, even if the crack tip advances. In conclusion, the fluctuation of K characterizes the cyclic stresses and strains in the near tip region of a propagating crack, even within r_p . This characterization is invariant to the planar geometry of a specimen if the condition of small scale yielding, SSY (i.e. $r_p \ll r_e$) is satisfied.

When a crack propagates under a constant ΔK (or under a slowly changing ΔK) at a given R-ratio, the value of ΔK alone will be able to characterize the cyclic stresses and strains in the near tip region. If the cyclic stresses and strains experienced by the materials control the crack growth rate, then one must conclude that

$$da/dN = f(\Delta K) \quad (2)$$

-4-

The stresses and strains are also affected by specimen thickness, t , and R-ratio. The functional relationship between da/dN and ΔK is affected by environment, cyclic frequency, ν , and testing temperature, T . Consequently, for a given material, one may write

$$da/dN = f(\Delta K, R, t, \nu, T, \text{ environment}) \quad (3)$$

This relation is true if $r_p \ll r_e$. r_e is linearly proportional to specimen size. Therefore, Equation (3) can always be made true, in principle, by using large enough samples. The SSY condition is the sufficient rather than the necessary condition. The necessary condition for Equation (3) is that a sample is large enough so that K characterizes the specific stress or strain component controlling the crack growth process.

The capability of ΔK to characterize cyclic strains in the near tip region was investigated by the moiré method and the results are given in the next section.

CYCLIC DEFORMATION IN CRACK TIP REGION [4]

The above analysis shows that under a constant ΔK (or slowly changing ΔK) fatigue loading, crack tip stresses and strains are characterized by ΔK . Besides ΔK , the stresses and strains are also affected by specimen thickness and R-ratio. Within the plastic zone in a thick specimen in the state of plane strain, the ratio between the maximum tensile stress and flow stress, $(\sigma_{\max}/\sigma_{\text{flow}})$ is approximately 2.45 under a static loading; and the ratio is nearly 1 for the state of plane stress. The strains in these two different states must vary accordingly.

The cyclic deformations in the crack tip regions at various K-levels were measured with the moiré technique [4]. Measurements were made on 2024-T351 aluminum center cracked plate specimens with a thickness of 6.4 mm and 1.28 mm (0.25" and 0.05") and R-ratios of 1/3 and 1/10. The static and cyclic yield strengths were 360 and 460 MPa (52 and 67 ksi) respectively, and the cyclic strain hardening exponent was 0.13.

As a fatigue crack propagates toward a material point far ahead of the tip, the cyclic strain at the point is, at first, elastic. As the tip gets closer to the point, the material at the point experiences plastic deformation during the loading half cycle, but the deformation is still elastic during the unloading half cycle. The plastic strain accumulates monotonically cycle after cycle as the tip propagates toward the point. As the crack tip moves even closer, plastic deformation takes place during the unloading as well as the loading half cycles, and the plastic deformation becomes cyclic. In a fatigue loading, there are monotonic plastic zone $r_{p(s)}$ and cyclic plastic zone, $r_{p(c)}$. The cyclic plastic zone is embedded within the monotonic plastic zone. Both the accumulated total strain, ϵ_{\max} , and the cyclic strain range, $\Delta\epsilon$, along the crack line were measured. From these strain measurements, the monotonic and cyclic plastic zones were determined [4].

The moiré patterns were obtained by the double exposure method. The specimen surface was coated with a photo-resist coating. The coating was first exposed to a high density moiré grille of 13,000 lpi, before the pre-cracked sample was loaded. The grille lines were parallel to the crack line to measure the displacement u_y . The second exposure was made at K_{\max} when the crack increment was long enough so that a "steady state" of cyclic plastic deformation at the crack tip region was realized. The moiré fringe pattern thus formed gave the total accumulated strain, ϵ_{\max} . After the picture of the fringe pattern was taken, the pattern was immediately removed, and a new photo-resist coating was applied to

measure cyclic strain range, $\Delta\epsilon$. Two exposures were made in succession, one each at K_{\min} and K_{\max} . The fringe pattern gave $\Delta\epsilon$.

-5-

The data of ϵ_{\max} and $\Delta\epsilon$ for the 1/4" thick specimens at $R=1/10$ are given in Figures 3 and 4. Additional data are given in Reference [4]. The data at a given ΔK - or K_{\max} -level in a logarithmic plot can be correlated very well by a straight line. For the ϵ_{\max} data, the slopes of the lines decrease from -0.5 at low K_{\max} levels to -0.8 at high K_{\max} levels.

Unfortunately, all the $\Delta\epsilon$ measurements were made outside the cyclic plastic zone. The moire pattern lost its definition when $r < 0.03$ ". However, all of the $\Delta\epsilon$ measurements were made within the monotonic plastic zone. The lines in the $\log \Delta\epsilon$ vs $\log r$ plot have a slope of -1/2, which agrees with the elastic calculation. If both σ_{xx} and σ_{yy} are taken into account,

$\epsilon_{yy} = (1 - \nu)\sigma_{yy}/E$. $\sigma_{yy}(r,0) = K/\sqrt{2\pi r}$. The measured $\Delta\epsilon_{yy}$ can be written as

$$\Delta\epsilon_{yy}(\text{measured}) = \beta \Delta\epsilon_{yy}(\text{theoretical}) = \beta \frac{(1-\nu)}{E} \frac{\Delta K}{\sqrt{2\pi r}} \quad (4)$$

The values of β are close to 1, and they are tabulated in Table I. The maximum deviation from the theoretical values is 35%. For a given combination of t and R , β is a constant.

TABLE I

t	R	$\beta = \frac{\Delta\epsilon_{\text{measured}}}{\Delta\epsilon_{\text{theoretical}}}$
1.27 mm (0.05")	1/10	1.06
1.27 mm (0.05")	1/3	1.18
6.35 mm (0.25")	1/10	1.25
6.35 mm (0.25")	1/3	1.35

The measured $\Delta\epsilon$ in the thin specimens is less than that in the thick specimens and is caused by crack closure in the thin specimens as will be explained later. $\Delta\epsilon$ is higher at a higher R -ratio. The higher $\Delta\epsilon$ is likely caused by cyclic creep, which is caused by the positive mean stress within $r_{p(C)}$.

The cyclic plastic zone size $r_{p(C)}$ can be obtained by extrapolating the measured $\Delta\epsilon$ line to a value of 9.3×10^{-3} , which corresponds to $2\sigma_{Y(C)} = 938$ MPa (134 ksi) with the Mises yield criterion. The monotonic plastic zone can be determined in a like manner. The results are shown in Figures 5 and 6. The dashed lines in these two figures are the calculated lines based on Irwin's plastic zone size formula. The larger measured plastic zone sizes in comparison with the calculated ones reflect the high measured strains.

Recognizing $2\sigma_{Y(C)}$ = yield stress range, at the initiation of the cyclic plastic deformation, we have,

$$\Delta\epsilon_{yy(Y)} = \frac{(1-\nu)}{E} 2\sigma_{Y(C)} = \beta \frac{(1-\nu)}{E} \frac{\Delta K}{\sqrt{2\pi r_{p(C)}}} \quad (5)$$

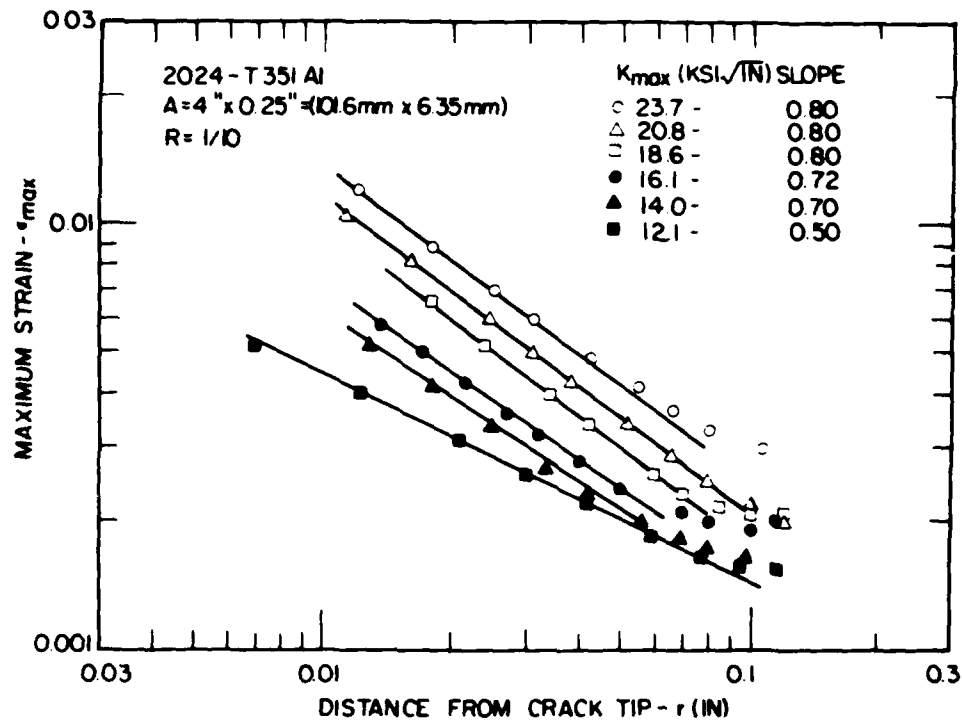


Fig. 3. Maximum strain distribution ahead of a crack tip for 6.35 mm thick 2024-T351 aluminum alloy at $R = 1/10$. Ref. [4a]

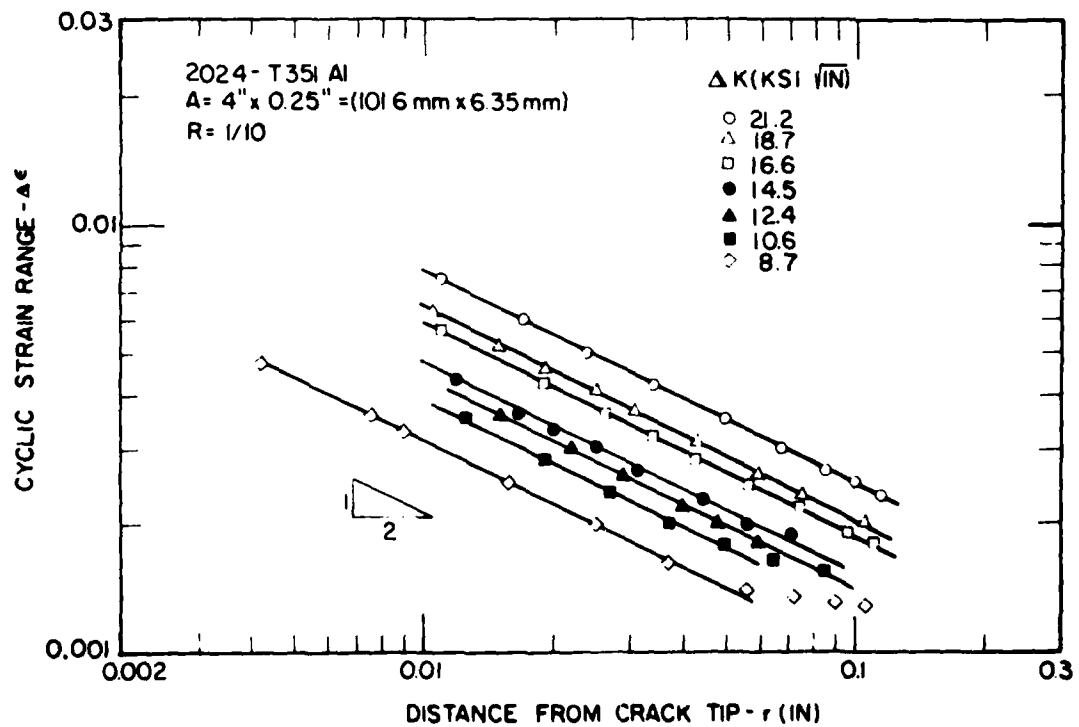


Fig. 4. Strain range distribution ahead of a crack tip for 6.35 mm thick 2024-T351 aluminum alloy at $R = 1/10$. Ref. [4a]

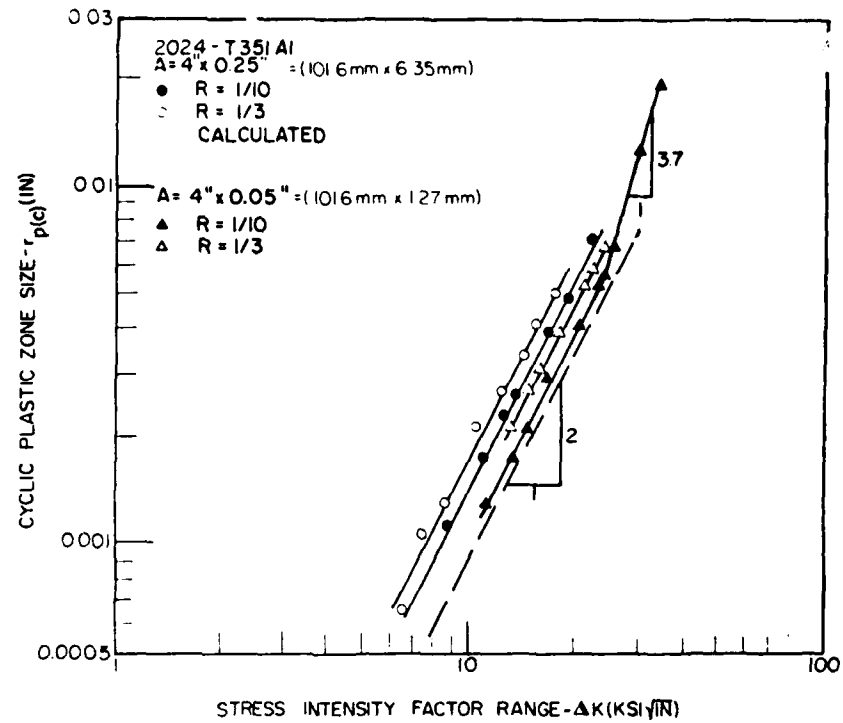


Fig. 5. Cyclic plastic zone size versus stress intensity factor range, Ref. [4b]

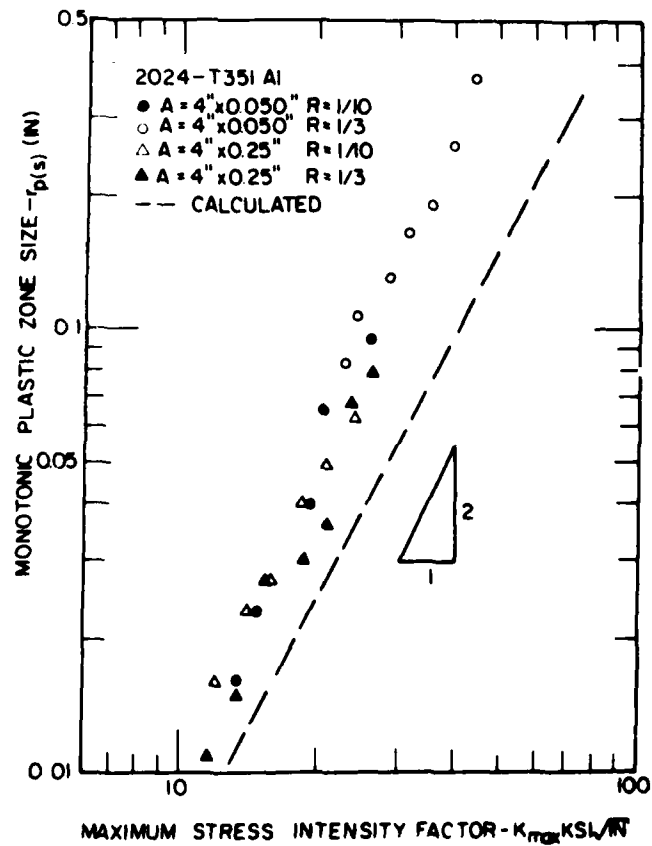


Fig. 6. Static plastic zone size versus the maximum stress intensity factor. Ref. [4b]

with $\Delta K^2 = E\Delta J$

-8-

$$r_{p(C)} = \frac{\beta^2}{2\pi} \left(\frac{\Delta K}{2\sigma_{Y(C)}} \right)^2 = \frac{\beta^2}{2\pi} \frac{E\Delta J}{(2\sigma_{Y(C)})^2} \quad (6)$$

Since all the $\Delta\epsilon$ lines are parallel and have the same slope of $-1/2$, the plot of all of the data of $\Delta\epsilon$ vs $r/r_{p(C)}$ fall on a single line. This is shown in Figure 7 for the 6.35 mm thick specimen at $R = 1/10$.

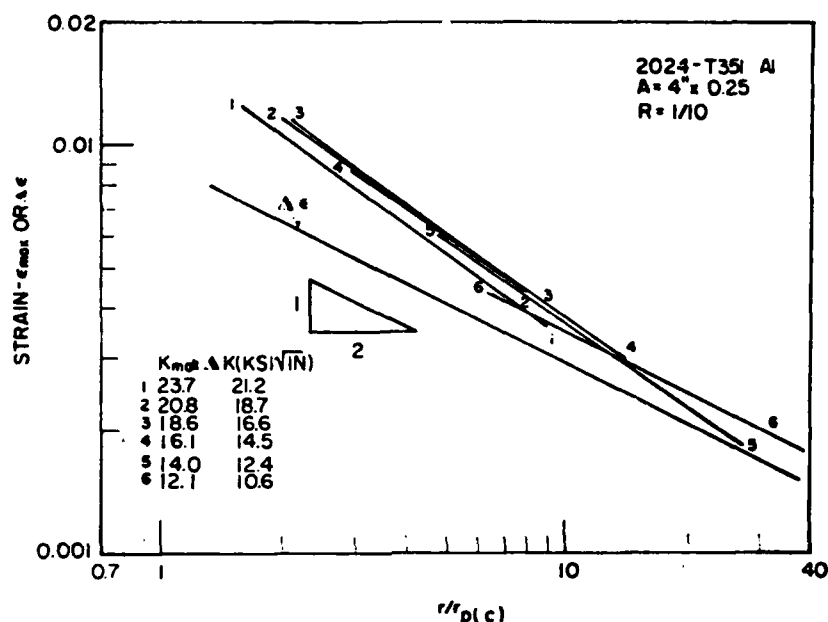


Fig. 7. Strain versus $r/r_{p(C)}$ for 6.35 mm thick specimens at $R = 1/10$. Ref. [4b]

Similarly, the ϵ_{max} data are plotted against $r/r_{p(C)}$ in the same figure. The ϵ_{max} data lie within a narrow band. The empirical relation

$$\epsilon_{max} = \alpha \left(\frac{r_{p(C)}}{r} \right)^m \quad (7)$$

correlates well with the data. ϵ_{max} can also be written as

$$\epsilon_{max} = \alpha \left(\frac{\beta^2}{2\pi} \frac{\Delta J}{2\sigma_{Y(C)}^2 \epsilon_{Y(C)} r} \right)^m \quad (8)$$

which is similar to that given by Hutchinsen [12], Rice and Rosengren [13]. For $t = 6.35$ mm and $R = 1/10$, the data in Figure 7 give $m = 0.8$ and $\alpha = 0.0045$. Additional data are shown in Figures 8, 9, and 10 for the other combination of t and R . ϵ_{max} is the highest for the thin specimens at the high R -ratio of $1/3$, and the lowest for the thick specimens at the low R -ratio of $1/10$. The other two sets of data are in between. The Moiré method measures the deformation on the surface of a specimen. The plastic deformation on the surface of a thick specimen is constrained by the interior of the specimen, where the deformation is in the

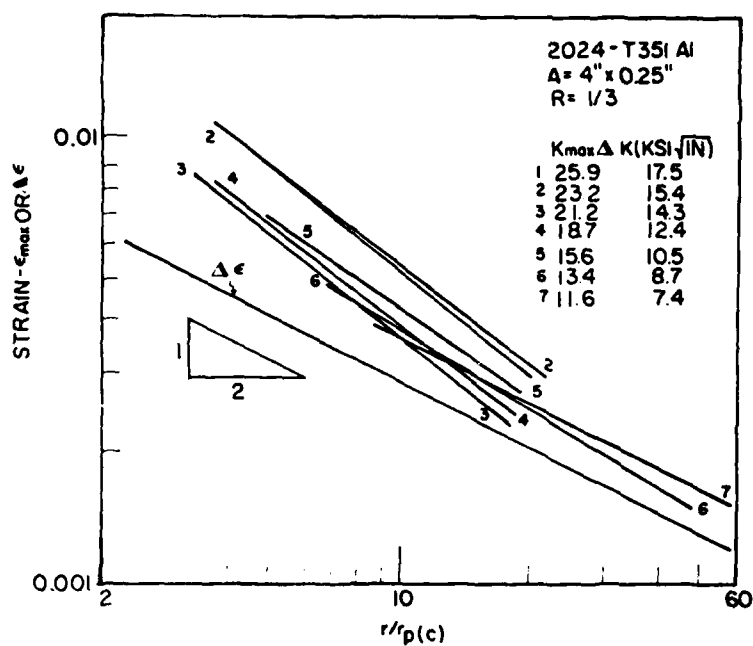


Fig. 8. Strain versus $r/r_p(c)$ for 6.35 mm thick specimens at $R = 1/3$. Ref. [4b]

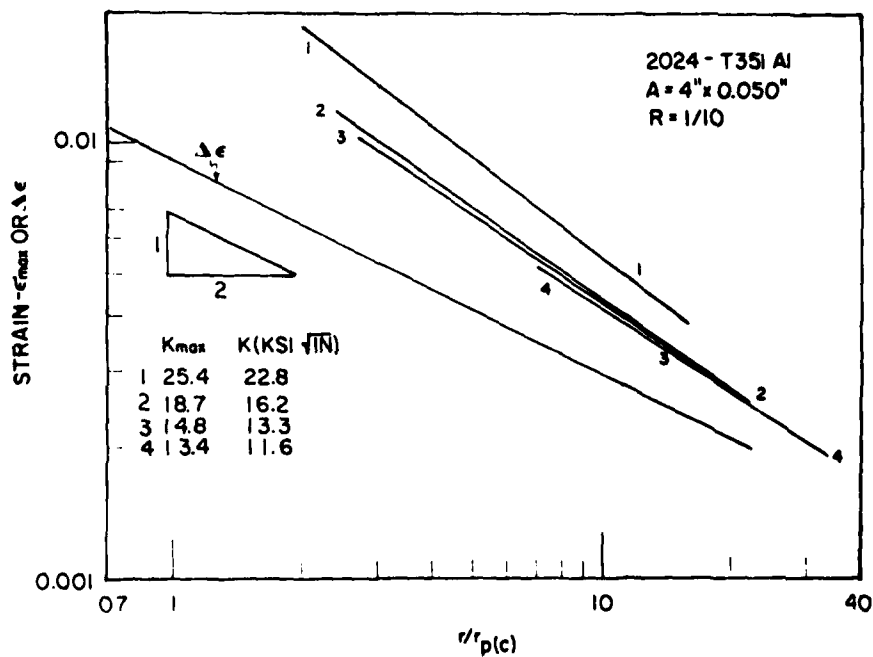


Fig. 9. Strain versus $r/r_p(c)$ for 6.35 mm thick specimens at $R = 1/10$. Ref. [4b]

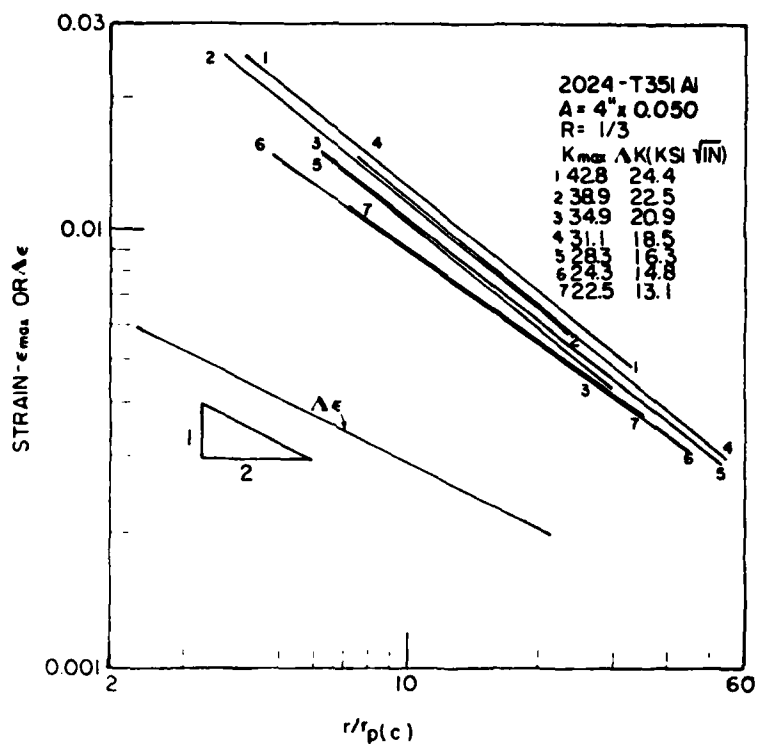


Fig. 10. Strain versus $r/r_p(c)$ for 1.27 mm thick specimens at $R = 1/3$. Ref. [4b]

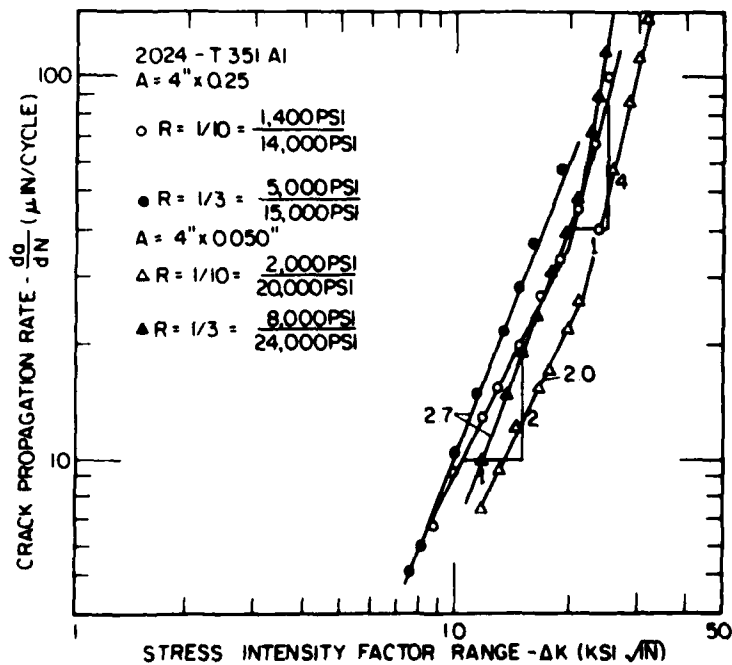


Fig. 11. Fatigue crack propagation rate for 2024-T351 aluminum alloy. Ref. [4b]

state of plane strain. On the surface of a thin specimen, the constraint is absent, and it is "free" to deform. Therefore ϵ_{\max} 's in thin specimens are higher -11- than those in thick specimens. The high measured ϵ_{\max} is also reflected in the large $r_{p(s)}$ in Figure 6.

Both cyclic creep and crack closure will affect the strains. At high R-ratio, the mean stress in the plastic zone is positive; the positive mean stress causes cyclic creep. Cyclic creep increases both $\Delta\epsilon$ and ϵ_{\max} at the higher R-ratio of 1/3 as shown in Table I and Figures 8, 9, and 10 and 11.

The increase in ϵ_{\max} is more pronounced in the thin specimens because of the lack of the constraint by the interior plane strain zone. The material within the plastic zone in thin specimens is stretched considerably more than that in the thick specimens. During the unloading, the highly stretched zone will cause crack closure and will reduce the effective ΔK . Therefore, $\Delta\epsilon$ in a thin specimen is less than that in a thick specimen as shown in Table I.

Figure 7 shows that all the $\Delta\epsilon$ data fall on a single line, therefore, $\Delta\epsilon$ can be expressed in terms of $r_p(C)$, which is in turn related to ΔK . Hence, $\Delta\epsilon$ can be directly related to ΔK . The ϵ_{\max} data fall within a narrow band ($\pm 5\%$). Therefore, ϵ_{\max} can also be expressed in terms of $r_p(C)$ and ΔK . At a given thickness and at a given R-ratio, ΔK can characterize both $\Delta\epsilon$ and ϵ_{\max} .

The ϵ_{\max} scatter bands for the other combinations of t and R are wider ($\pm 15\%$) as shown in Figures 8, 9, and 10. If the lines for the three high K_{\max} values are eliminated from Figures 8 and 9, the scatter band is reduced considerably. The possible causes for data scatter include the thumb nail configuration of the internal crack front, and the shift of the crack to the shear plane at the high K_{\max} levels. The shift reduced plane strain constraint and caused an increase in plastic strain.

The fatigue crack growth data in Figure 11 show that the crack growth rate increases in the same order as the increase in $\Delta\epsilon$, that is in the order of $R = 1/10$, $t = 1.27$ mm; $R = 1/3$, $t = 1.25$ mm; $R = 1/10$, $t = 6.35$ mm; and $R = 1/3$, $t = 6.35$ mm.

In conclusion: ΔK characterizes both $\Delta\epsilon$ and ϵ_{\max} in a crack tip region and the cyclic strains are affected by both specimen thickness and R-ratio. Since fatigue crack growth is closely related to plastic deformation, therefore da/dN must be related to ΔK , t , and R .

THE UNZIPPING MODEL OF FATIGUE CRACK GROWTH

Orowan [5] has proposed the alternating shear rupture on two sets of intersecting slip planes as the ductile fracture mechanism. Subsequently, crack tip blunting by shear decohesion has been proposed as the mechanism for fatigue striation formation and fatigue crack growth [6,7,8]. Neumann [8] has directly observed alternating shear rupture, which causes crack tip opening and crack growth in copper single crystals under cyclic loading.

Plastic deformation in single crystals is not continuous as has been assumed in continuum mechanics. Rather, it concentrates in discrete parallel slip bands separated by crystal layers, which are essentially elastic as shown in Figure 12. The same deformation processes may also occur at the crack tip in a crystalline solid. The slip bands in a single crystal coincide with the slip planes of the crystal. The deformation in the slip band of a polycrystal are the result of a number of active slip systems of each crystal in a band, and the slip bands coincide with the plane of maximum shear stresses. Figure 13 shows two sets of parallel intersecting slip bands at a crack tip. As the applied stress increases, shear decohesion takes place alternately on slip bands 1, 2, 3, and 4, in

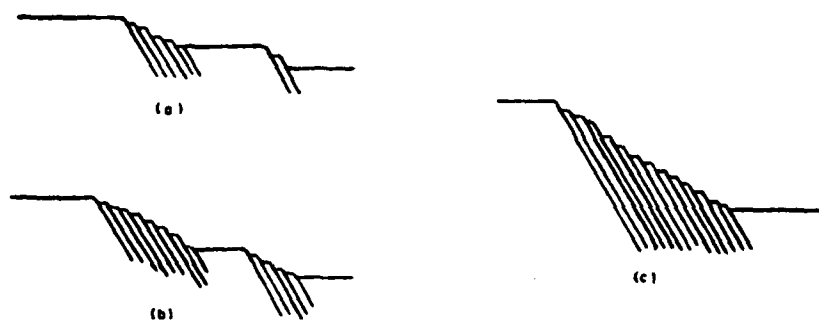


Fig. 12. Development of laminar slip bands with increasing deformation, (a) and (b), and laminae at high deformation (c), Ref. [1].

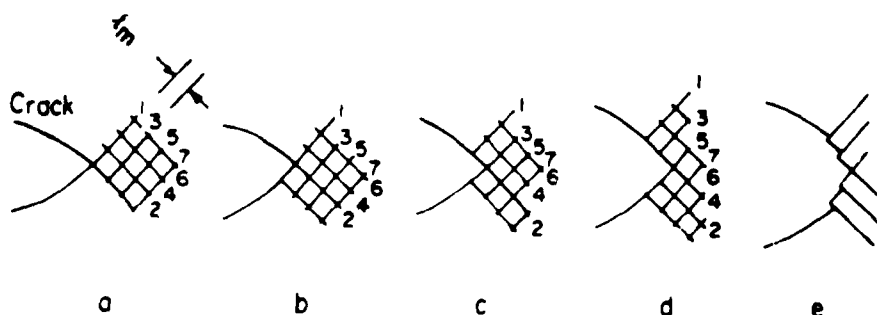


Fig. 13. The unzipping model for crack opening and advance.

succession. The elastic slabs between the neighboring slip bands move away from the crack tip, one at a time, like the teeth of a zipper during the unzipping process. As the slabs move, the crack tip opens up, and the crack moves forward.

Kuo and Liu [9] have modelled the crack tip unzipping process using the finite element method. A cracked circular solid is loaded with boundary displacement excitation as shown in Figure 14a. The solid is loaded incrementally to a predetermined K-level. The stresses and strains are calculated, and the plastic zone, r_p , is delineated. At the K-level, a slip band such as AB is chosen, Figure 14b. Each of the nodal points along AB is branched into two. A small load increment, δK is then applied. During the increment, the branched nodal points are allowed to slide freely along AB, but they are not allowed to move away from AB. In the meantime, plastic deformation is allowed to occur to all the elements during δK . The crack increment caused by the unzipping process, $\delta \Delta a_{uz}$, during the increment δK is calculated.

According to the dimensional analysis and the results of the past studies, the unzipping crack increment must be

$$\Delta a_{uz} = C(1-\nu^2) \frac{K^2}{E\sigma_Y} \quad (9)$$

where C is an unknown proportional constant; ν is the Poisson's ratio; E is the Young's modulus; and σ_Y is the yield stress. Differentiating both sides, one obtains

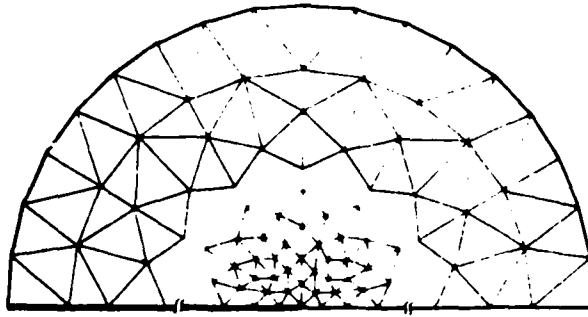


Fig. 14a. Finite element configuration, $\beta = 45^\circ$.

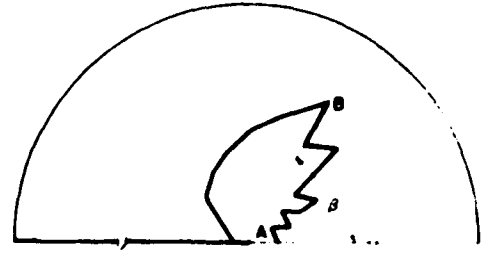


Fig. 14b. Plastic zone and decohesion plane.

$$\delta \Delta a_{uz} = C(1-\nu^2) \frac{2K\delta K}{E\sigma_Y} \quad (10)$$

The values of K , δK , and $\delta \Delta a_{uz}$ from the finite element calculation enable us to evaluate C . Thus we have

$$\Delta a_{uz} = 0.04 (1-\nu^2) \frac{K^2}{E\sigma_Y} = \frac{0.04J}{\sigma_Y} \quad (11)$$

where $J = (1 - \nu^2)K^2/E$. Yang [14] repeated the calculations for a cracked circular solid and, in addition, has made a calculation for a compact tension specimen. His results are essentially the same

Under a fatigue load, as the applied load increases from K_{min} , the stresses at any point within the cyclic plastic zone, $r_{p(C)}$ increase. The plastic deformation at the point takes place when the effective stress increases by the amount of $2\sigma_{Y(C)}$, instead of σ_Y as in the static case. Therefore, one can justifiably use Equation (11) to calculate fatigue crack growth rate with the substitutions of da/dN , ΔK , and $2\sigma_{Y(C)}$ for Δa_{uz} , K , and σ_Y respectively. After these substitutions, one obtains

$$\frac{da}{dN} = 0.02 (1-\nu^2) \frac{\Delta K^2}{E\sigma_{Y(C)}} = 0.02 \frac{\Delta J}{\sigma_{Y(C)}} \approx 0.018 \frac{\Delta K^2}{E\sigma_{Y(C)}} \quad (12)$$

Bates and Clark [15] related fatigue striation spacing with ΔK for a number of materials. Taking striation spacing as da/dN , we have

$$\frac{da}{dN} = 6 \left(\frac{\Delta K}{E} \right)^2 \quad (13)$$

From the available literature, Hahn et al. [16] have correlated da/dN with ΔK for a number of steels. They found that

$$\frac{da}{dN} = 8 \left(\frac{\Delta K}{E} \right)^2 \quad (14)$$

Pook and Frost [17] have found a similar relation

$$\frac{da}{dN} = \frac{9}{\pi} \left(\frac{\Delta K}{E} \right)^2 \quad (15)$$

Barsom [18] tested the fatigue crack growth of a number of steels. He found

-14-

$$\frac{da}{dN} = 0.66 \times 10^{-8} \Delta K^{2.25} \text{ (inches/cycle)} \quad (16)$$

According to Bates and Clark, Hahn et al., and Pook and Frost, da/dN can be written as

$$\frac{da}{dN} = C \left(\frac{\Delta K}{E} \right)^2 \quad (17)$$

With $\sigma_{Y(C)}/E = 1/400$ and $E = 207 \times 10^6 \text{ MPa} = 30 \times 10^6 \text{ psi}$ for steel, the empirical equations and the theoretical equation are plotted in Figure 15. The agreement is very good.

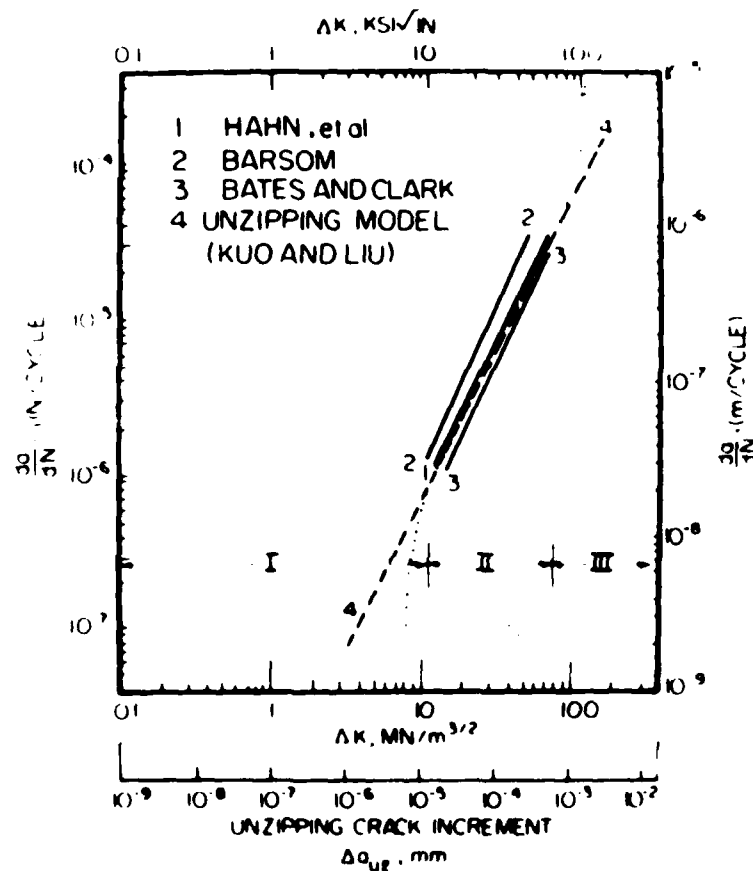


Fig. 15. Comparison of the empirical fatigue crack growth rates in steels with that predicted by the unzipping model. Ref. [11]

The measured crack growth data of various steels do not seem to vary much. It is known that the cyclic yield strengths of steels do not vary much because the annealed soft steels usually cyclically harden, and hardened steels usually cyclically soften. The value of the ratio $\sigma_{Y(C)}/E$ does not vary much from one

steel to another. If their crack growth is controlled by the deformation process, their growth rates should not vary much either.

-15-

Kobayashi et al. [19] measured the striation spacings of a variety of metals and alloys. The measured striation spacings are related to $\Delta J/\sigma_{\text{flow}}$ as shown in Figure 16. For a number of materials, $\sigma_{\text{flow}} < 2 \sigma_{Y(C)} < 2 \sigma_{\text{flow}}$. Two

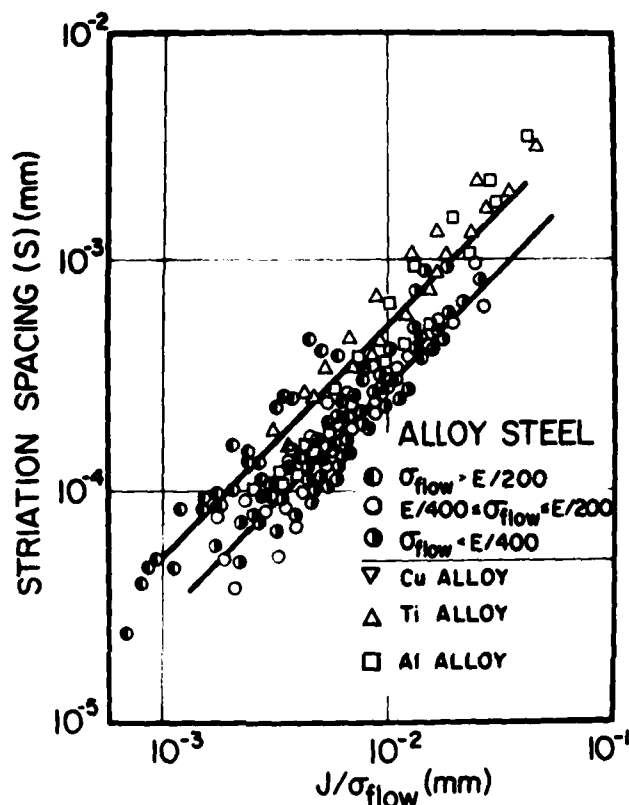


Fig. 16. Comparison of striation spacing with that predicted by the unzipping model. Ref. [20]

lines in Figure 16 are calculated according to Equation (12) with $2 \sigma_{Y(C)} = \sigma_{\text{flow}}$ for one line and $\sigma_{Y(C)} = \sigma_{\text{flow}}$ for the other. Again the agreement is very good. More detailed discussions of the modelling and the comparison with the experimental results are given by Kuo and Liu [9], Liu, Yang, and Kuo [3], and Liu and Kobayashi [20].

In the unzipping model, the crack growth rate is much less than that given by the Dugdale strip yielding model. As a crack tip is deformed and blunted during a rising load, the crack tip opens up and the tip grows forward. However, only part of the blunting crack opening displacement contributes to crack growth.

Figure 17a shows slip band A at a crack tip. As K increases, the shear decohesion at A causes crack tip blunting and crack growth as shown in Figure 17b. As the crack tip grows during a rising K , the slip band A is left behind. The slip band A will continue to be active. Once behind the crack tip, the shear decohesion at A will blunt the crack tip but will not contribute toward crack growth as shown in Figure 17c.

Let $\delta K_1 = (K_1 - 0)$; $\delta K_2 = (K_2 - K_1)$;; $\delta K_n = (K_n - K_{n-1})$. Along the

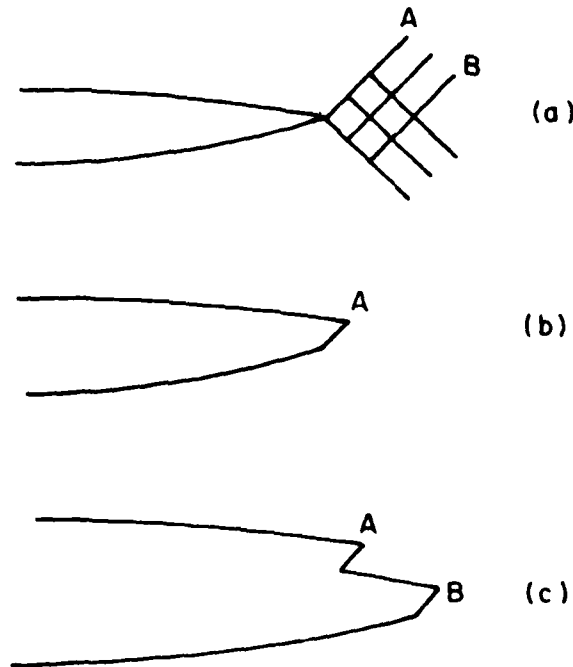


Fig. 17. Shear decohesion, crack tip blunting, and crack growth.

crack path, n slip bands will participate in the unzipping process. After δK_p , the crack tip reaches the slip band $(P+1)$. During each of the δK_n increments, shear decohesions take place on all of those slip bands at or behind the crack tip. All of these shear displacements will blunt the crack tip, but only the opening displacement on the slip band at the crack tip contributes to crack growth. Let $\delta CTOD_{mp}$ be the crack tip opening displacement, which takes place on slip band m during the increment δK_p . $\delta CTOD_{mp}$ are tabulated below.

	Slip Band 1	Slip Band 2	Slip Band n
δK_1	$\delta CTOD_{11}$		
δK_2	$\delta CTOD_{12}$	$\delta CTOD_{22}$	
\vdots	\vdots	\vdots	
\vdots	\vdots	\vdots	
δK_n	$\delta CTOD_{1n}$	$\delta CTOD_{2n}$	$\delta CTOD_{nn}$

The crack growth is the sum of the diagonal terms. The crack blunting and Dugdale CTOD include not only the off-diagonal terms but also the shear deformation along the crack flank which is behind the original crack tip at the beginning of a loading cycle. Therefore, the crack growth rate calculated with the Dugdale model is nearly ten times greater than the experimental values.

In the calculation, the slip step size, $\delta \Delta a_{uz}$, is assumed to be very small. The model is valid even if the slip step is equal to one atomic spacing.

Slip bands can easily be seen on the surface of a plastically deformed crystal. Intense plastic deformation takes place on certain parallel slip planes, while the layers of the crystal between these active slip planes remain practically undeformed, as illustrated in Figure 12. In aluminum, the thickness of the undeformed crystal layer, is about 200 Å [1]. Let the minimum thickness of the crystal layer be ℓ_m . When the unzipping crack increment Δa_{uz} is less than ℓ_m , the applied load will reverse the slip direction before the crack front reaches the intersecting conjugate slip plane β as shown by the dashed line, position 2 in Figure 18b. Upon unloading, however, the crack tip

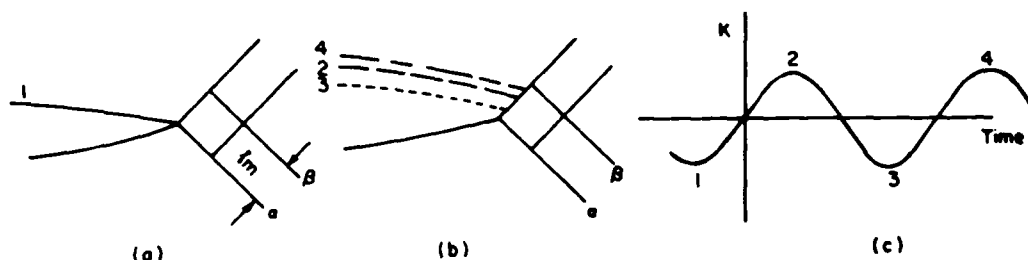


Fig. 18. Cyclic creep shear decohesion when $\Delta a_{uz} < \ell_m$. Successive positions of the upper crack surface during a stress cycle are indicated. The additional shear decohesion between positions 2 and 4 is caused by cyclic creep.

will not return to its original location. The mean shear stress on the slip plane, $(\tau_{max} - \tau_{min})/2$ lies in the direction to open the crack tip. During the next loading cycle, the mean shear stress will cause "cyclic creep" slip, moving the crack tip a little closer to the conjugate slip plane β , position 4 in Figure 18b. Additional shear decohesion between positions 2 and 4 is caused by cyclic creep. This cyclic creep slip motion will continue during the subsequent loading cycles, until the crack front reaches the slip plane β . Then, the unzipping process will switch to the conjugate plane. A large number of cycles is needed to propagate the crack by the amount of ℓ_m . Therefore, when crack growth rate is less than ℓ_m , the growth rate decreases drastically with ΔK . This is known commonly. This crack growth rate transition takes place at $da/dN \sim \ell_m$ and at $\Delta K = \Delta K_t$.

Below the transition point, the size of the crack growth "step" remains constant, equal to ℓ_m . But it takes a large number of cycles to propagate a crack through ℓ_m . Hertzberg and Mills [21] have observed constant crack growth step in aluminum, stainless steel, brass, and Ni-Cb eutectic composite. Constant growth step size were observed over two decade range of crack growth rates. Similar observations have been made by Gell and Leverant [22].

The sharp decrease in crack growth rate as ΔK decreases, often occur in the neighborhood of 200 Å/cycle, ($\sim 10^{-6}$ inches/cycle), a value close to the observed ℓ_m for aluminum. The crack growth step size observed by Hertzberg and Mills is likely to be $2\ell_m$ consisting of one step on one slip plane and another on the conjugate slip plane.

The transition point, ΔK_t , is given by

$$\ell_m = 0.018 \frac{\Delta K_t^2}{E\sigma_y(C)} \quad (18)$$

When cyclic creep takes place, the mean stress is relaxed. When the mean stress is relaxed, two effects will increase shear decohesion. First, as the mean stress relaxes to zero, a part of the elastic strain at K_{\max} is converted to plastic strain and shear decohesion. Second, when the stress relaxation takes place, the flow stress at K_{\max} is reduced. This reduction in flow stress will increase the plastic zone size and increase plastic deformation and shear decohesion. A rigorous evaluation of the stress relaxation and cyclic creep shear decohesion is difficult especially if the discrete deformation mechanism is taken into consideration. However, the end results of these two effects can be considered as the reduction of $\sigma_{Y(C)}$ in the calculation of Δa_{uz} .

When stress relaxation takes place, the flow stress at K_{\max} decreases. Figure 19 illustrates the stress relaxation at a point cycled within a fixed strain

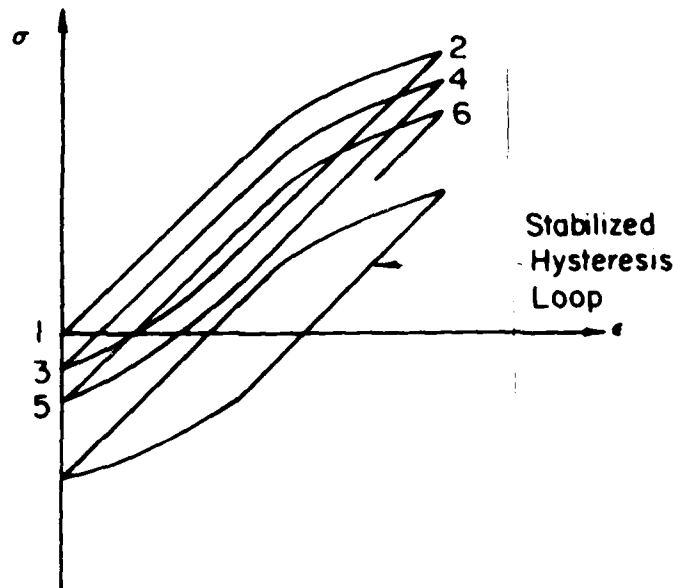


Fig. 19. Relaxation of mean stress and stabilized hysteresis loop. Successive stress reversals are numbered.

range, $\Delta \epsilon$. The σ_{\max} decreases cycle by cycle until the mean stress is relaxed to zero and σ_{\max} is nearly the half of the value at the beginning of the cycle loading. Figure 19 illustrates the stress relaxation where plastic deformation takes place during both loading and unloading half cycles. In this case, the rate of relaxation is rather fast. However, the stress relaxation within the cyclic plastic zone is coupled to the slow relaxation within the monotonic plastic zone, where relaxation takes place only when the stress deviates slightly from the elastic deformation during the re-loading half cycle. The rate of unzipping cyclic creep shear decohesion is directly related to the overall relaxation rate. When the mean stress is relaxed to zero, the flow stress is reduced approximately by half. Thus we have

$$\Delta a_{uz} = 0.018 \frac{\Delta K^2}{E(\sigma_{Y(C)}/2)} \quad (19)$$

When the cyclic creep shear decohesion is taken into consideration, if Δa_{uz} is

still less than ℓ_m , the crack tip will move back and forth between two neighboring conjugate slip bands, and the crack will remain dormant. Therefore ΔK becomes ΔK_{th} . Combining Equations (18) and (19), we have

$$\Delta K_{th} \approx 0.7 \Delta K_t \quad (20)$$

$$\Delta J_{th} \approx 0.5 \Delta J_t \quad (21)$$

Figure 20 shows the data of A533B steel [23]. The values of ΔJ_t and ΔJ_{th} are 18 in-lb/m² and 36 in-lb/m², and the ratio $\Delta J_t / \Delta J_{th}$ is 0.5 as given in Equation (20).

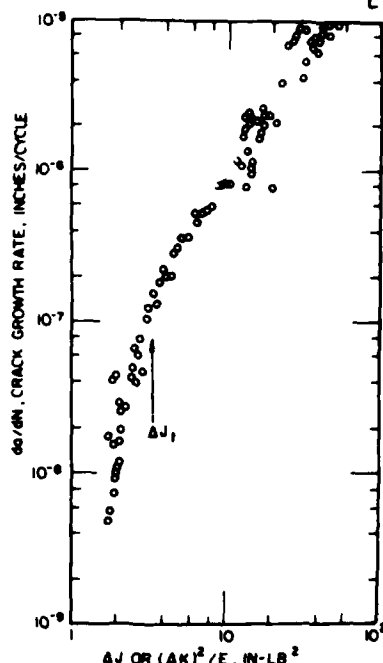


Fig. 20. Fatigue crack growth rate of A533B steel versus ΔJ . Data from Ref. [23]

The cyclic creep shear decohesion model for ΔK_{th} takes the deformation process into consideration. It is well known that ΔK_{th} is environmentally sensitive. The chemical effects must be superimposed onto the deformation mechanism. The details remain to be studied. However, the relation $\Delta K_{th} = 0.7 \Delta K_t$ seems valid for a number of materials tested in detrimental chemical environments.

THE GROWTH OF FATIGUE MICRO-CRACKS

When a crack is very small, the applied stress is often high. It is often close to or even higher than the yield stress of the material, in order to keep ΔK above ΔK_{th} . In this situation, the linear elastic fracture mechanics is no longer applicable. Yang and Liu [10] have used the finite element method to model the unzipping crack growth process in a single edge-cracked plate with an applied stress up to the yield stress. The unzipping crack increment is given by

$$\Delta a_{uz} = \int_0^K \frac{d\Delta a_{uz}}{dK} dK \quad (22)$$

At various K -levels, the quantity $d\Delta a_{uz}/dK$ was calculated, and Δa_{uz} was obtained by numerical integration. The calculated crack growth rate is

$$\frac{da}{dN} = (0.018 + 0.020 \frac{\Delta\sigma}{\sigma_{Y(C)}}) \frac{\Delta K_{appa}^2}{E \sigma_{Y(C)}} \quad (23)$$

where $\Delta\sigma$ is the applied stress range and ΔK_{appa} is the apparent ΔK value obtained from the linear elastic solutions. In the case of small scale yielding, the ratio $\Delta\sigma/\sigma_{Y(C)}$ approaches zero, and Equation (23) is reduced to Equation (12). ΔK_{eff} is the ΔK -value corresponding to Δa_{uz} in the small scale yielding case. Combining Equations (12 and 23), we have

$$\left(\frac{\Delta K_{eff}}{\Delta K_{appa}}\right)^2 = \frac{\Delta J_{eff}}{\Delta J_{appa}} = 1 + 1.11 \frac{\Delta\sigma}{\sigma_{Y(C)}} \quad (24)$$

In the intermediate crack growth rate region, Δa_{uz} corresponds directly to da/dN . In the lower ΔK region near the threshold, da/dN is much less than Δa_{uz} , because of the discrete nature of the crack growth process. However, in this region, we can use Δa_{uz} as a physical parameter that characterizes the crack tip shear decohesion process as illustrated in Figure 15. This is analogous to the use of elastic ΔK to characterize crack tip stress and strains even if plastic deformation takes place.

When a nucleated micro-crack is at the threshold of crack growth, ΔK_{eff} becomes ΔK_{th} , and the applied stress amplitude ($\Delta\sigma/2$) becomes the endurance limit, σ_e . ΔK_{th} is related to $\Delta a_{uz(th)}$ by Equation (12). $\Delta a_{uz(th)}$ is used here as a physical parameter that characterizes the shear decohesion process at a crack tip for crack growth threshold. With $\Delta K_{appa} = 1.1 \Delta\sigma\sqrt{\pi a}$ for a single-edge-cracked plate and "a" as the crack nucleus size, a_n , we have

$$\frac{\Delta a_{uz(th)}}{a_n} = \frac{\pi \sigma_{Y(C)}}{E} (0.09 + 0.20 \frac{\sigma_e}{\sigma_{Y(C)}}) \left(\frac{\sigma_e}{\sigma_{Y(C)}}\right)^2 \quad (25)$$

Equation (25) relates endurance limit to crack nucleus size, a_n and $\Delta a_{uz(th)}$. The crack nucleus size a_n is dictated by the nucleation process. For example, if a fatigue crack is nucleated by an inclusion particle, a_n must be related to the size of the particle.

FATIGUE CRACK GROWTH IN A FERRITIC-MARTENSITIC TWO PHASE STEEL

The fatigue crack growth behaviours of martensitic-ferritic steel have been studied [24,25,26,27]. Fatigue cracks in such steels are often nucleated in the soft ferrite region. If the applied stress is high enough, the nucleated cracks will propagate across the martensite to the final failure.

Yang and Liu [11] analyzed the unzipping crack growth process by using the finite element method. The two phase structure is simulated by a thin layer of ferrite over a martensite core as shown in Figure 21. The quantity, $d\Delta a_{uz}/dK$ is calculated at various K-levels, and the crack growth rate is obtained by numerical integration. The results of the calculation are shown in Figure (22) for three stress ranges: $\Delta\sigma = 690, 550$, and 410 MPa (100, 80, and 60 ksi). The unzipping crack increment, Δa_{uz} can be considered as the crack growth rate. It can also be used as a physical parameter to characterize crack tip shear decohesion process.

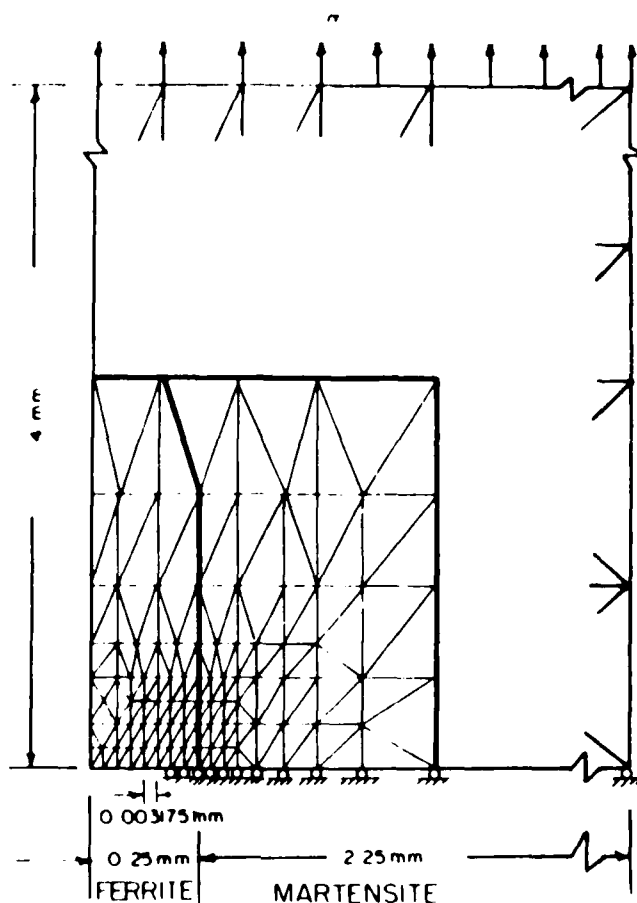


Fig. 21. Finite element mesh represents a two-phase martensitic-ferritic steel.

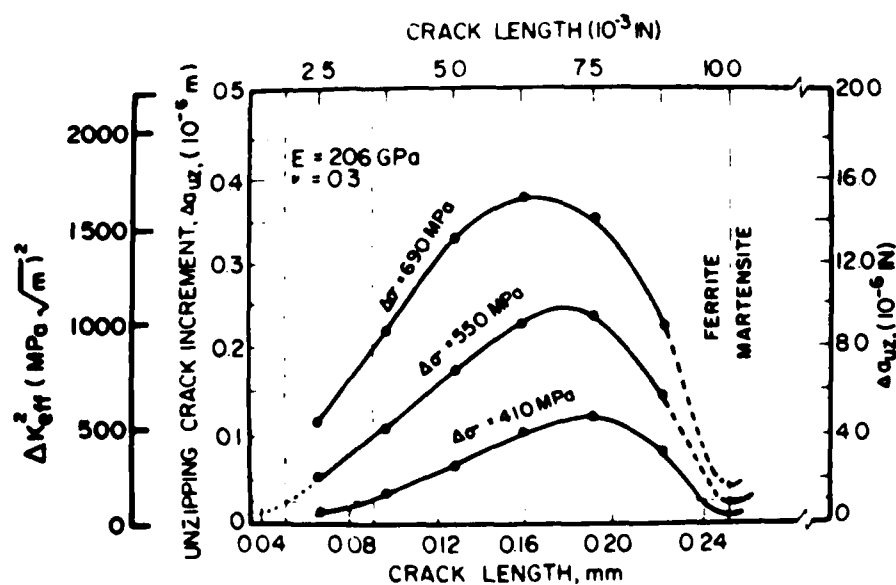


Fig. 22. Unzipping increment obtained by FEM simulation. [11]

At a given applied $\Delta\sigma$ -level, before the plastic zone touches the ferrite-martensite interface boundary, $\Delta\sigma_{uz}$ increases with crack length a . When the plastic zone reaches the interface, the hard martensite constrains the plastic

deformation in the ferrite. Therefore, the rate of increase of Δa_{uz} decreases. A maxima is reached, and Δa_{uz} decreases as the crack tip approaches the interface. This variation of the calculated Δa_{uz} agrees with the crack growth data in Figure 23. The growth rate increases initially. However, the growth rate

-22-

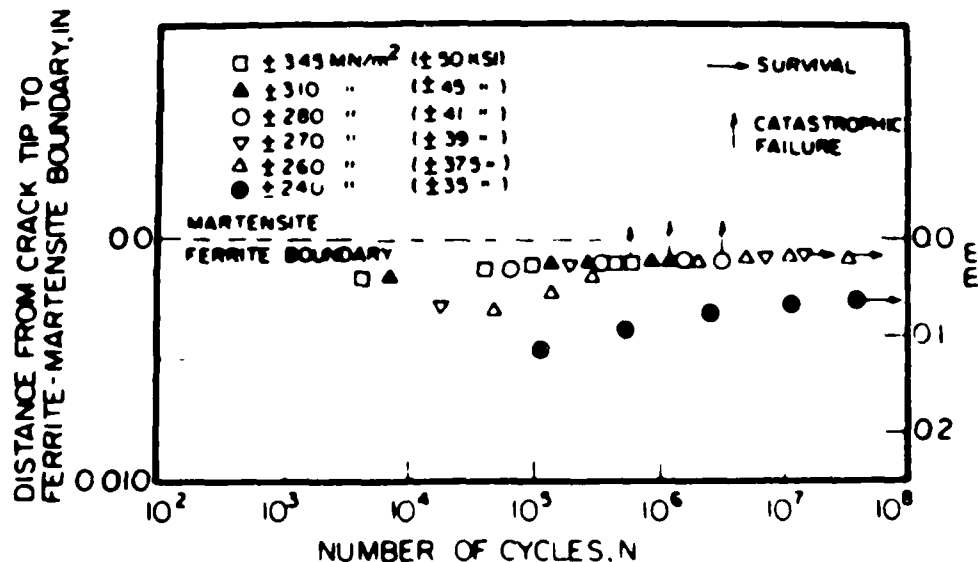


Fig. 23. Fatigue crack growth in a ferritic-martensitic steel. Ref. [23]

decreases as the crack tip approaches the interface. If the applied stress is low, and ΔK_{eff} is below ΔK_{th} , a crack may even be stopped within the ferrite region. ΔK_{th} is directly related to $\Delta a_{uz(th)}$. Therefore, the threshold condition can also be characterized by $\Delta a_{uz(th)}$. The qualitative agreement between the calculation and the experiment is very good. An improved calculation, using the actual material properties of the ferrite and the martensite, is needed for quantitative comparisons.

A QUANTITATIVE ANALYSIS OF MICRO-STRUCTURE AND FATIGUE LIMIT

In order to have fatigue failure in a two phase steel, a crack has to be nucleated, and the applied stress has to exceed the threshold for the propagation of the nucleated micro-crack. The crack nucleus in the soft ferrite has to overcome the constraint of the hard martensite; the crack has to penetrate the ferrite-martensite interface. Once in the martensite, the crack has to overcome the cracking resistance, ΔK_{th} , of the martensite. The fatigue limit of the steel can be controlled by any one of these processes.

If the crack nucleus sizes, the crack nucleation stresses the thresholds for fatigue crack growth in ferrite and martensite and the cyclic yield strengths of ferrite and martensite, and in addition the thickness of the ferrite layer are known. The fatigue limit of a two phase steel can be evaluated quantitatively.

First, consider the ferrite alone without the complication of the martensite. Let the stress for crack nucleation be σ_n . The value of σ_n and a_n will give us the value of ΔK_{eff} . Equation (24). If $\Delta K_{eff} > \Delta K_{th(ferrite)}$ the crack will continue to grow until failure. Therefore, the fatigue limit σ_e is equal to σ_n , and σ_e is controlled by the crack nucleation process.

If ΔK_{eff} at σ_n is less than $\Delta K_{th}(\text{ferrite})$, the nucleated crack will stay dormant, until the applied stress is increased. Therefore, $\sigma_e > \sigma_n$ and the fatigue limit is controlled by the crack propagation process. -23-

The relation between crack nucleus size and fatigue limit is given by Equation (25). For the ferrite, we assume $\sigma_{Y(C)} = 380$ MPa, $\pi\sigma_{Y(C)}/E = 5.8 \times 10^{-3}$, and $\Delta a_{uz(th)} = 28 \times 10^{-6}$ mm, which corresponds to $\Delta K_{th} = 11 \text{ MPa}\sqrt{\text{m}}$. The calculated relation between a_n and σ_e is plotted in Figure 24. σ_e changes from 200 to 300 MPa as a_n varies from 0.085 to 0.03 mm.

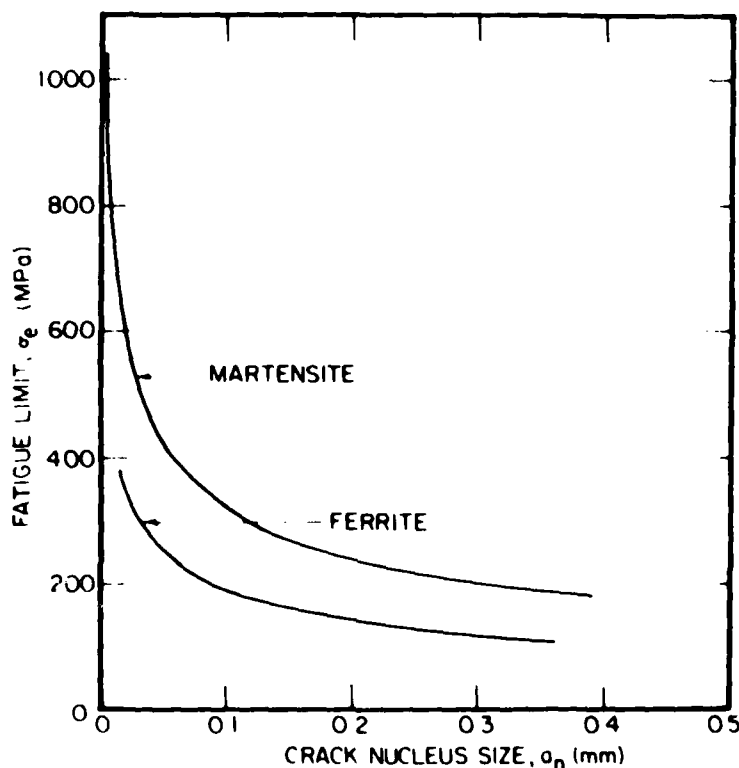


Fig. 24. Crack nucleus size and fatigue limit.

The curve for the martensite is also plotted in the figure. For the martensite, we assume $\Delta a_{uz(th)} = 23 \times 10^{-6}$ mm, which corresponds to $\Delta K_{th} = 16.5 \text{ MPa}\sqrt{\text{m}}$. $\sigma_{Y(C)} = 1035$ MPa, and $E = 207,000$ MPa. The fatigue limit of the martensite changes from 600 to 800 MPa as the crack nucleus size varies from 0.02 to 0.01 mm.

Once a crack grows into the martensite, if the applied ΔK is less than $\Delta K_{th}(\text{martensite})$, the crack will stop propagating. The fatigue limit is thus controlled by the cracking resistance of the martensite. With the crack length equal to the ferrite layer thickness, the fatigue limit can be calculated with Equation (12 or 25). For a single edge-cracked plate, and for $\Delta K_{th}(\text{martensite}) = 16.5 \text{ MPa}\sqrt{\text{m}}$, the fatigue limit of the two phase steel is plotted in Figure 25.

The fatigue limits controlled by crack non-propagation in both martensite and ferrite are also plotted in the figure. For the ferrite, $\sigma_e = 300$ MPa and $a_n = 0.03$ mm; and for the martensite, $\sigma_e = 800$ MPa and $a_n = 0.01$ mm.

When a crack tip grows close to the ferrite-martensite interface, the unzipping crack increment, Δa_{uz} decreases as shown in Figure 22. When the shear

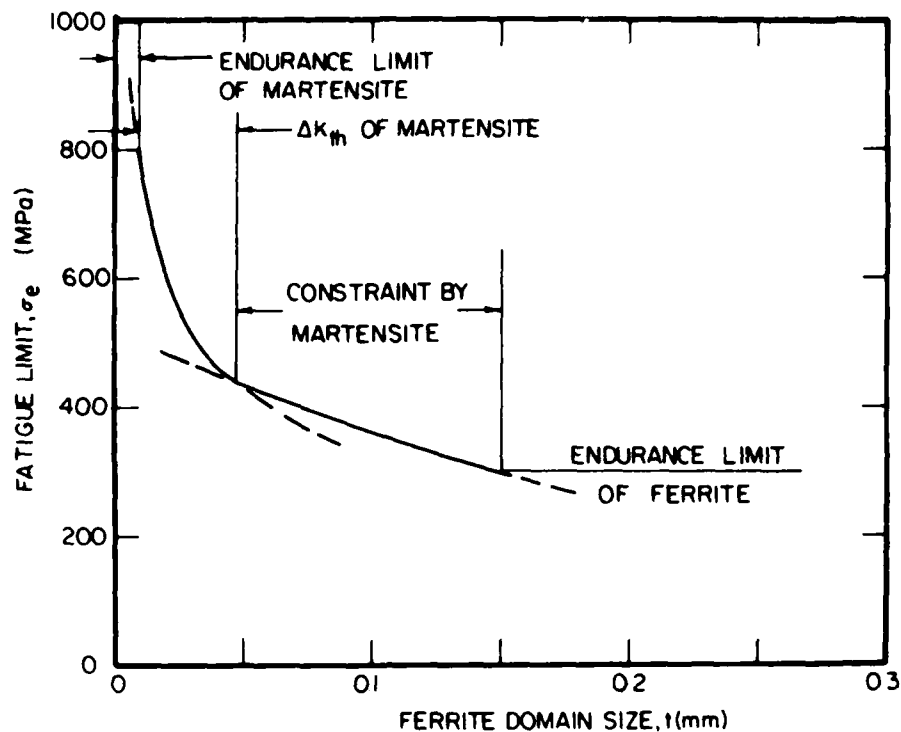


Fig. 25. Fatigue limit and ferrite domain size.

decohesion increment decreases below $\Delta a_{uz(th)}$ for crack growth threshold, the crack stops in the ferrite region as shown by the three specimens at the lower stress levels in Figure 23.

The unzipping crack increment calculation as shown in Figure 22 could be used to construct the relation between the fatigue limit of the steel and the ferrite domain size, when martensite constraining is the controlling process. However, a much finer finite element mesh is needed to establish the quantitative relation. The line in Figure 25 is a schematic line.

Figure 25 gives an overall view of the fatigue limit of the steel. The effects of crack nucleus size in the ferrite and the martensite, the crack growth thresholds of the ferrite and the martensite, the stress necessary for crack nucleation, and the ferrite domain size are all intimately related to the fatigue limit. Such an analysis will help to optimize the micro-structures in order to achieve the best fatigue strength.

This analysis illustrates the need to study the effects of large scale yielding, the discrete nature of plastic deformation, and the material inhomogeneity in order to establish the quantitative relation between fatigue strength and micro-structure.

DISCUSSIONS

Fatigue crack growth rate are often correlated with ΔK . If the specimen is large enough and the applied load is low enough so that the condition of small scale yielding prevails, ΔK is capable of characterizing crack tip stresses and cyclic plastic strains. In other words, a given value of ΔK corresponds uniquely to a state of crack tip stresses and strains. If fatigue crack growth is the result of cyclic stresses and cyclic strains at the tip, da/dN must be related uniquely to ΔK . When the condition of small scale yielding is not met, a given value of ΔK may result in a number of different states of crack tip stresses and strains. Therefore, ΔK is no longer able to correlate with da/dN . In the case

of large scale yielding, both Δa_{uz} and ΔJ are applicable.

-25-

ΔK and ΔJ are applicable as long as they can characterize crack tip stresses and strains. Both ΔK and ΔJ are used as indirect parameters, which do not infer any crack growth mechanisms. Nor the growth mechanism need to be known in order to make such correlations.

In the case of the ferritic-martensitic two phase steel, neither ΔK nor ΔJ is capable to characterize the crack tip stresses or strains. Therefore, neither ΔK nor ΔJ can be used to correlate crack growth rate. Δa_{uz} is equal to da/dN ; therefore it is a direct parameter for crack growth correlation. A direct parameter, if known, is always preferred because it has a much wider range of applicability.

Mechanical metallurgy studies the mechanical properties as affected by microstructures. In the stress analysis, neither discrete plastic deformation nor material inhomogeneity are taken into consideration. Fatigue crack growth is the direct result of the discrete plastic deformation process. A quantitative relation can be derived directly only if the discrete deformation process is taken into consideration.

It is suggested to develop a new field of study of metallurgical mechanics, which takes inhomogeneity, anisotropy, and the discrete deformation process into account in the stress analysis. Then, use the calculated local stresses and strains to correlate with microstructures. This paper illustrates such studies on the effects of discrete slip process and the effects of material inhomogeneity on crack growth. The recent developments in mechanics and metallurgical studies set the stage for fruitful efforts and rapid progress in this area.

CONCLUSIONS

1. Cyclic plastic deformation at a crack tip may cause a fatigue crack to grow. In the case of small scale yielding, ΔK is able to characterize the cyclic plastic deformation at a crack tip, and ΔK can be used to correlate with da/dN successfully.
2. The unzipping model of fatigue crack growth agrees with the measured crack growth rate and striation spacing measurements.
3. The unzipping model is extended to micro-cracks and the ferritic-martensitic two-phase steel.
4. ΔK and ΔJ are indirect parameters to correlate da/dN .
5. Neither ΔK nor ΔJ can be used to study the micro-structural effects on da/dN . In this case, a direct parameter, such as Δa_{uz} is needed.
6. A model of crack growth threshold is proposed. The model predicts correctly the crack growth behavior in the near threshold region.
7. A quantitative analysis on microstructure and fatigue limit is illustrated. Such quantitative analysis will help to optimize the micro-structures to achieve high fatigue strength.

ACKNOWLEDGEMENT

This paper synthesizes the earlier works on fatigue crack growth conducted at Syracuse University. The crack tip strains were measured by Dr. Tai Shan Kang, the unzipping model of fatigue crack growth was made by Dr. Alber S. Kuo and the unzipping model was extended to micro-cracks and ferritic-martensitic steel by Dr. C. Y. Yang. The financial supports by NASA Grant NGR-33-022-105; NSF Grant No. GK34047 and ARO DAAG29-78-G0069 are acknowledged.

REFERENCES

1. Heidenreich, R. D. and Shockley, W., "Study of Slip in Aluminum

Crystals by Electron Microscope and Electron Diffraction Methods," Rep. of a Conf. on Strength of Solids, Phys. Soc. London, 1948, pp. 57-75.

2. Liu, H. W., "Analysis of Fatigue Crack Propagation," NASA Contract Report, NASA CR-2032, May 1972.

3. Liu, H. W., Yang, C. Y., and Kuo, A. S. Cyclic Crack Growth Analysis and Modelling of Crack Tip Deformation," International Symposium of Fracture Mechanics, George Washington University, Washington, D.C., U.S.A., Sept. 1978.

4. Kang, Tai Shan, "Fatigue Crack Tip Deformation and Fatigue Crack Propagation," Ph.D. Dissertation, Solid State Science and Technology, Syracuse University, Syracuse, N.Y., 1972.

5. Orowan, E., "Fracture and Strength of Solids," Rep. Prog. Phys. (12), 1949, pp. 185-232.

6. Laird, C., "The Influence of Metallurgical Structure on the Mechanisms of Fatigue Crack Propagation," ASTM STP 415, Fatigue Crack Propagation, 1967, pp. 131-180.

7. Pelloux, R. M. N., "Mechanism of Formation of Ductile Fatigue Striations," Trans. ASM 62, 1969, pp. 281-285.

8. Neumann, V. P., "New Experiments Concerning the Slip Processes at Propagating Fatigue Cracks - I, II," Acta Met. 22, 1974, pp. 1155-1178.

9. Kuo, A. S. and Liu, H. W., "An Analysis of Unzipping Model for Fatigue Crack Growth," Scripta Met., Vol. 10, 1976, pp. 723-728.

10. Yang, C. Y. and Liu, H. W., "The Application of Unzipping Model of Fatigue Crack Growth to Micro-Cracks," Scripta Met. Vol. 15, 1981, pp. 507-512.

11. Yang, C. Y. and Liu, H. W., "The Unzipping Model of Fatigue Crack Growth and Its Application to a Two-Phase Steel," Int. J. of Fracture, Vol. 17, No. 2, April 1981.

12. Hutchinson, J. W., "Singular Behavior at the End of a Tensile Crack in a Hardening Material," J. of Mech. and Phys. of Solids, Vol. 16, 1968, pp. 13-31.

13. Rice, J. R. and Rosengren, A. F., "Plane Strain Deformation Near a Crack Tip in a Power Law Hardening Material," J. of Mech. and Phys. of Solids, Vol. 16, 1968, pp. 1-12.

14. Yang, C. Y., "Modelling of Crack Tip Deformation with Finite Element Method and Its Application," Ph.D. Dissertation, Solid State Science and Technology, Syracuse University, Syracuse, N.Y., 1979.

15. Bates, R. C. and Clark, W. G., Jr., "Fractography and Fracture Mechanics," Trans. ASM, Vol. 62, 1969, pp. 380-389.

16. Hahn, G. T., Hoagland, R. C., and Rosenfield, A. R., AF 33615-70-C-1630 Battelle Memorial Inst., Columbus, Ohio, August, 1971.

17. Frost, N. E., Marsh, K. J., and Pook, L. P., "Metal Fatigue," Clarendon Press, Oxford, 1974.

18. Barsom, J. M., "The Dependence of Fatigue Crack Propagation on Strain Energy Release Rate and Crack Opening Displacement," ASTM STP 486, Damage Tolerance in Aircraft Structures, 1971, pp. 1-15.

19. Kobayashi, H., Nakamura, H., and Nakazawa, H., "The Relation Between Crack Tip Plastic Blunting and the J-integral," Proceedings 3rd Int. Conf. on Mech. Behavior of Materials, Pergamon Press, 3, 1979, p. 529.

20. Liu, H. W. and Kobayashi, H., "Stretch Zone Width and Striation Spacing-The Comparison of Theories and Experiments," Scripta Met., Vol. 16, May 1980.

21. Hertzberg, R. W. and Mills, W. J., "Character of Fatigue Fracture Surface Micromorphology in the Ultra-low Growth Rate Regime," Fractography - Microscopic Cracking Processes, ASTM STP 600, Am. Soc. for Testing and Materials, 1976, pp. 220-234.

22. Gell, M. and Leverant, G. R., "The Fatigue of the Nickel-Base Superalloy, MAR-M200, in Single-Crystal and Columnar-Grained Forms at Room Temperature," Transaction, Am. Inst. of Mining, Metallurgical and Petroleum Engineers, Vol. 242, 1968, 1869.

23. Dowling, N. E. and Begley, J. A., ASTM STP 590, 1976, pp. 82-103.

24. Kunio, T. and Yamada, K., "Microstructural Aspects of the Threshold Condition of Non-Propagating Fatigue Cracks in Martensitic-Ferritic Structure," Symposium on the Fatigue Mechanisms, Kansas City, Missouri, 1978.

25. Kunio, T., Shimizu, M., Yamada, K., and Suzuki, H., "An Effect of the Second Phase Morphology on the Tensile Fracture Characteristics of Carbon Steels," Engineering Fracture Mechanics, Vol. 7, 1975, pp. 411-417.

26. Suzuki, H. and McEvily, A. J., "Microstructural Effects on Fatigue Crack Growth in a Low Carbon Steel," Met. Trans. A 10-No. 4, April 1979, pp. 475-482.

-27-

27. Minakawa, K. and McEvily, A. J., "On the Influence of Microstructure on the Threshold Level for Fatigue Crack Growth in Steels," to be published.

APPENDIX III

LIST OF PUBLICATIONS

- W. Hu, S. Kuo and H. W. Liu, "A Study on Crack Tip Deformation and Ductile Fracture", Proceedings of 12th Annual Meeting of Soc. of Eng. Science, Austin, Texas (1975).
- W. L. Hu and H. W. Liu, "Crack Tip Strain - A Comparison of FEM Calculations and Measuremnts", Proceedings of the Ninth National Symposium of Fracture Mechanics, Pittsburgh, Pa., August 1975, ASTM STP 601, Crack and Fracture (1976)
- W. L. Hu and H. W. Liu, "Characterization of Crack Tip Stresses and Strains - Small Scale Yielding and General Yielding", Proceedings of the Second Intl. Conference on Mechanical Behavior, August 16-20, 1976, Boston, Mass.
- H. W. Liu and C. Y. Yang, "Strip Yielding Model and Fracture Toughnesses of Thin and Tough Plates," Proceedings of International Conference - Fracture Mechanics in Engineering Application, Bangalore, India, March 26-30, 1979.
- H. W. Liu, Thickness Effects on Fracture Criteria," U.S.-Japan Joint Seminar on "Fracture Mechanics of Ductile and Tough Materials and Its Application to Energy Related Structures," Kanazawa, Japan, Nov. 1979 (To be published in the Proceedings).
- H. W. Liu and H. Kobayashi, "Stretch Zone Width and Striation Spacing - The Comparison of Theories and Experiments," Scripta Met. Vol. 14, May 1980.
- H. W. Liu, W. L. Hu and A. S. Kuo, "Thickness Effects on the Choice of Fracture Criteria", ASTM Second International Symposium on Elastic-Plastic Fracture Mechanics, Philadelphia, PA, October 6-9, 1981, To be published in the proceedings.
- H. W. Liu, "Crack Tip Deformation and Fatigue Crack Growth", Mechanics of Fatigue, AMD-Vol. 47, Edited by T. Mura, November 1981.

APPENDIX IV

LIST OF STUDENTS SUPPORTED BY THE GRANT

Dr. Wan-lian Hu - "A Finite Element Study on Crack Tip Deformation"
Westinghouse Corporation, Richland, Washington

Dr. Chuang-Yeh Yang - "Modelling of Crack Tip Deformation with Finite Element
Method and Its Applications"
Westinghouse Corporation, Monroeville, Pennsylvania

Mr. Chien-Erh Hong - "Rigid Body Bending and Crack Opening Displacement"
Intel Corporation, Aloha, Oregon

DATE
FILMED
- 8